

Dominant NNLO corrections to four-fermion production near the W -pair production threshold

S. ACTIS, M. BENEKE, P. FALGARI, C. SCHWINN

*Institut für Theoretische Physik E, RWTH Aachen University,
D-52056 Aachen, Germany*

Abstract

We calculate the parametrically dominant next-to-next-to-leading order corrections to four-fermion production $e^-e^+ \rightarrow \mu^- \bar{\nu}_\mu u \bar{d} + X$ at centre-of-mass energies near the W -pair production threshold employing the method of unstable-particle effective theory. In total the correction is small, leading to a shift of 3 MeV in the W -mass measurement. We also discuss the implementation of realistic cuts and provide a result for the interference of single-Coulomb and soft radiative corrections that can easily be extended to include an arbitrary number of Coulomb photons.

1 Introduction

W -pair production at e^-e^+ colliders is a key process for measuring the W -boson mass and testing the non-abelian structure of the Standard Model (SM), because of its sensitivity to triple non-abelian gauge couplings. The total cross section has been measured at LEP2 in a kinematical region spanning from the W -pair production threshold to a centre-of-mass energy of 207 GeV [1] with an accuracy of $\sim 1\%$ at the highest energies. The W mass has been determined with an error of ~ 40 MeV reconstructing the W bosons from their decay products; bounds on possible anomalous couplings are less stringent, and deviations from the SM predictions have been constrained at the per-cent level. A detailed analysis of the W -pair production process will be possible at the planned International Linear Collider, where the total cross section could be measured at the per-mille level [2]. The precision on the W -mass determination has been estimated to be ~ 10 MeV by a direct reconstruction of the W -decay products [3], and ~ 6 MeV by a dedicated threshold scan [4]. Moreover, the possibility to scan the high-energy region would allow to measure more precisely the size of the triple non-abelian gauge couplings.

The estimates on the W -mass determination rely on statistics and the performance of the future linear collider, and they assume that the cross section can be predicted by theory to sufficient accuracy in order to convert its measurement into one for the W mass. For this reason, radiative corrections to on-shell W -pair production have been thoroughly investigated in the past and are known at next-to-leading order (NLO) since the beginning of the 1980's [5]. However, the W bosons being unstable, a precise theoretical prediction has to be formulated for a final state of stable or sufficiently long-lived particles, represented by the fermion pairs produced by W decay, rather than for on-shell W bosons. NLO predictions for four-fermion production far from the W -pair threshold region are available since some time in the double-pole approximation [6, 7, 8] or with further simplifications [9, 10]. Recently, a full NLO computation of four-fermion production has been performed in the complex-mass scheme [11, 12] without any kinematical approximation; moreover, a compact analytic result around the threshold region has been obtained in [13] using effective field theory (EFT) methods [14, 15, 16].

In particular, the analysis performed in [13] led to the following conclusions: 1) a resummation of next-to-leading collinear logarithms from initial-state radiation is mandatory to reduce the error on the W mass from the threshold scan below ~ 30 MeV; 2) the NLO partonic cross-section calculation in the EFT approach implies a residual error of $\sim 10 - 15$ MeV. Although a large component of the uncertainty at point 2) can be removed using the full NLO four-fermion calculation [11, 12], the computation of the dominant higher order corrections, whose contribution has been estimated to be roughly ~ 5 MeV in [13], is necessary to secure the 6 MeV accuracy goal [4].

In this paper we employ EFT techniques to calculate analytically the (parametrically) dominant next-to-next-to-leading order (NNLO) corrections to the inclusive four-fermion production process $e^-e^+ \rightarrow \mu^-\bar{\nu}_\mu u\bar{d} + X$, where X stands for an arbitrary flavour-singlet state, with a three-fold goal: to improve the EFT NLO calculation [13]; to derive a result which can be added on top of the full NLO prediction [11, 12]; to reduce the uncertainty on the W -mass measurement below the required 5 MeV level by including a new set of higher order corrections.

The organisation of the paper is as follows. In section 2 we outline the structure of our computation, review the essential features of the EFT method and identify the set of parametrically leading NNLO corrections. In section 3 we describe in detail the calculation of the various contributions. In section 4 we show the numerical impact of our result on the inclusive

cross section and in section 5 we discuss the effect of realistic cuts adopting those applied at LEP2 as a template. As a by-product we explain how invariant-mass cuts can be included in the EFT approach. Finally, section 6 contains our conclusions and two appendices collect results related to the renormalisation of the Coulomb potential and the electromagnetic coupling, and the conversion from the fixed-width to the complex-mass scheme.

2 Outline of the computation

We consider the inclusive four-fermion production process

$$e^-(p_1) e^+(p_2) \rightarrow \mu^- \bar{\nu}_\mu u \bar{d} + X, \quad (1)$$

where X denotes an arbitrary flavour-singlet state (nothing, photons, gluons, ...), in the kinematical regime close to the W -pair production threshold, $s \equiv (p_1 + p_2)^2 \sim 4 M_W^2$. Here the total cross section is dominated by the production of two resonant non-relativistic W bosons with virtuality of order $k^2 - M_W^2 \sim M_W^2 v^2 \sim M_W \Gamma_W \ll M_W^2$, where v is the non-relativistic velocity and M_W and Γ_W are the W pole mass and decay width. We recall that the relation between the pole mass and the value given by experimental collaborations $\hat{M}_W = (80.403 \pm 0.029) \text{ GeV}$ [17] is given by $\hat{M}_W - M_W = \Gamma_W^2 / (2M_W) + \mathcal{O}(\alpha_{ew}^3)$ [18], where $\alpha_{ew} \equiv \alpha / s_w^2$, α is the fine-structure constant, $s_w^2 \equiv \sin^2 \theta_w$ and θ_w denotes the weak-mixing angle.

In the framework of unstable-particle effective field theory (EFT) [14, 15, 16] the total cross section is obtained through a re-organised loop expansion and a kinematical expansion in the small parameters

$$\alpha_{ew}, \quad \frac{s - 4 M_W^2}{4 M_W^2} \sim v^2, \quad \frac{\Gamma_W}{M_W} \sim \alpha_{ew}. \quad (2)$$

All three parameters are of the same order, and in the following we will denote them as δ for power-counting purposes. Obviously, the EFT expansion is not equivalent to a standard loop expansion; in particular, being tailored to a specific kinematical region, it allows for a straightforward evaluation of leading higher order corrections. In order to appreciate this point, let us briefly review how the EFT exploits the hierarchy of scales and deals with the threshold region. The key observation consists in recognising four momentum scalings in the centre-of-mass frame, in the spirit of the method of regions [19],

$$\begin{aligned} \text{hard : } & k_0 \sim |\vec{k}| \sim M_W, & \text{potential : } & k_0 \sim M_W \delta, \quad |\vec{k}| \sim M_W \sqrt{\delta}, \\ \text{soft : } & k_0 \sim |\vec{k}| \sim M_W \delta, & \text{collinear : } & k_0 \sim M_W, \quad k^2 \sim M_W^2 \delta, \end{aligned} \quad (3)$$

where k is an arbitrary loop-integration momentum. Starting from NNLO diagrams another mode has to be included in addition to the ones given in (3) that will be called¹ ‘semi-soft’:

$$\text{semi-soft : } k_0 \sim |\vec{k}| \sim M_W \sqrt{\delta}. \quad (4)$$

Hard modes are integrated out, and their contribution is encoded in appropriate matching coefficients. The remaining dynamical modes appear in genuine EFT loop computations and their different scaling properties lead to a non-standard power counting in the small expansion parameter δ involving half-integer powers.

¹This is analogous to the ‘soft’ mode in the NRQCD literature whose ‘ultrasoft’ mode corresponds to the ‘soft’ mode in our conventions.

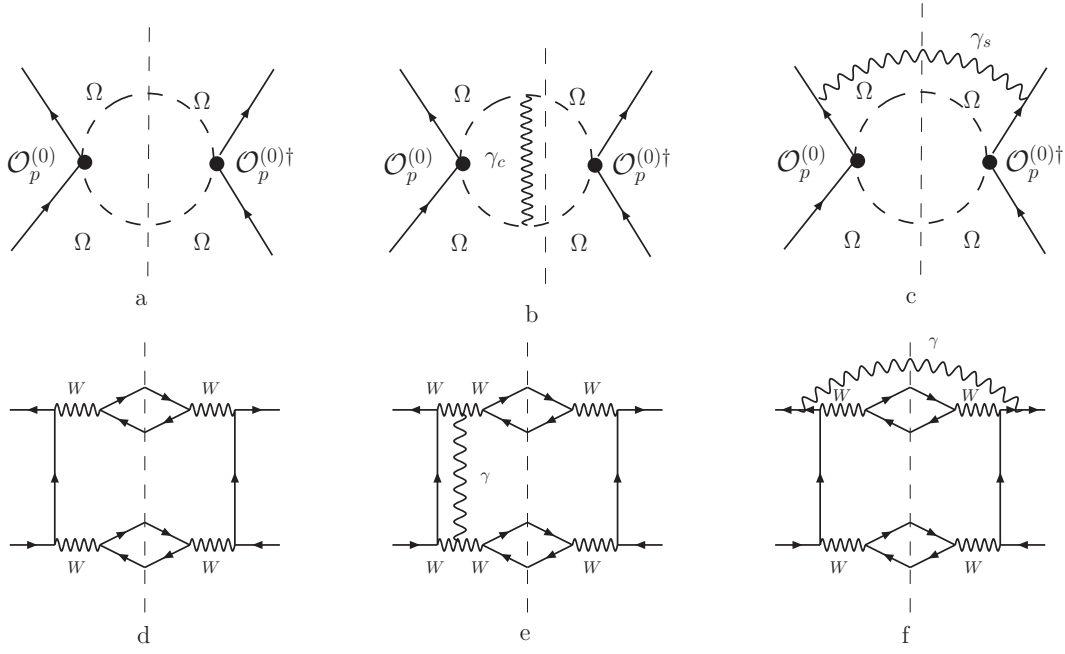


Figure 1: Sample diagrams in the EFT (first line) and in the full SM (second line). External fermionic lines are electrons and positrons; internal fermionic lines appearing in the diagrams in the second line represent the $\mu^- \bar{\nu}_\mu$ and $u \bar{d}$ doublets.

The total cross section of (1) is related through unitarity to the appropriate cuts of the $e^- e^+$ forward-scattering amplitude. Figure 1d shows a sample diagram contributing to the cut forward-scattering amplitude in the full Standard Model (SM). In the EFT language, the leading-order (LO) EFT contribution to the forward-scattering amplitude for the helicity configuration $e_L^- e_R^+$, the only non-vanishing one at LO in the non-relativistic expansion, reads

$$i\mathcal{A}_{LR}^{(0)} = \int d^4x \langle e_L^- e_R^+ | T[i\mathcal{O}_p^{(0)\dagger}(0) i\mathcal{O}_p^{(0)}(x)] | e_L^- e_R^+ \rangle. \quad (5)$$

The corresponding cut diagram is illustrated in figure 1a. Here the operators $\mathcal{O}_p^{(0)}$ and $\mathcal{O}_p^{(0)\dagger}$ account at LO for the production and destruction of a pair of non-relativistic W bosons. Their explicit expressions are given by

$$\mathcal{O}_p^{(0)} = \frac{\pi \alpha_{ew}}{M_W^2} \left(\bar{e}_{c2,L} \gamma^{[i} n^{j]} e_{c1,L} \right) \left(\Omega_-^{\dagger i} \Omega_+^{\dagger j} \right), \quad (6)$$

where we have introduced the short-hand notation $a^{[i} b^{j]} \equiv a^i b^j + a^j b^i$. Here \vec{n} represents the unit vector for the direction of the incoming electron three-momentum \vec{p}_1 , γ^i , with $i = 1, 2, 3$, are the usual Dirac matrices, the subscripts on the electron fields denote the two different direction labels of the collinear fields and Ω_\pm^i , with $i = 1, 2, 3$, are non-relativistic spin-1 destruction fields for particles with electric charge ± 1 , whose propagators are

$$\frac{i \delta^{ij}}{k^0 - \frac{|\vec{k}|^2}{2M_W} + \frac{i\Gamma_W}{2}}. \quad (7)$$

Loop corrections to the unstable-particle EFT scattering amplitude are then computed using the vertex (6), the propagator (7) and interactions with potential photons, related to the Coulomb force between the slowly-moving W bosons, (semi-) soft, and collinear photons.

For definiteness, let us consider selected radiative corrections to the LO EFT cut diagram from figure 1a, and show how the non-standard power counting arises. From the scaling properties (3), it is clear that the propagators (7) of the potential fields Ω scale as $1/\delta$ and the integration measure $d^4 k$ as $\delta^{5/2}$; since each vertex (6) contains the coupling constant α_{ew} , we can associate a power-counting factor $\alpha_{ew}^2 \delta^{1/2}$ to the LO diagram.

We now turn to virtual Coulomb (potential) corrections, shown in figure 1b, where we denote the loop momentum of the Coulomb photon by k_c . The corresponding SM diagram is depicted in figure 1e. The photon propagator scales as $1/\vec{k}_c^2 \sim 1/\delta$ and the integration measure $d^4 k_c$ as $\delta^{5/2}$; including the overall factor $\alpha \sim \delta$ due to the photon interaction vertices and two additional W propagators, we obtain a power-counting factor $\alpha_{ew}^2 \delta$. The situation is quite different for the soft real-photon corrections illustrated in figure 1c (see figure 1f for the Standard Model counterpart). The photon propagator, parametrised by the loop momentum k_s , scales as $1/k_s^2 \sim 1/\delta^2$, and the integration measure $d^4 k_s$ as δ^4 ; each collinear internal fermion line scales as $1/(k_s \cdot p_i) \sim 1/\delta$, with $i = 1, 2$, where p_1 and p_2 are the incoming momenta of the external electron and positron; the two photon vertices introduce an overall factor $\alpha \sim \delta$; the power-counting factor associated to the soft-photon diagram is $\alpha_{ew}^2 \delta^{3/2}$.

The standard loop expansion of figure 1e and figure 1f treats virtual Coulomb corrections and real soft-photon contributions as genuine NLO effects. The re-organised EFT expansion, instead, shows that Coulomb-photon corrections at the W -pair production threshold are suppressed with respect to the LO diagram by a factor $\delta^{1/2}$, and can be classified as dominant effective $N^{1/2} \text{LO}^{\text{EFT}}$ terms in the small expansion-parameter δ ; soft-photon corrections are suppressed by one power of δ , and can be treated as sub-dominant NLO^{EFT} effects.

The aim of this paper is to calculate corrections to the four-fermion production cross section which are not included in the SM NLO result, but might be relevant to the W mass analysis at the 5 MeV level. It is therefore natural to turn our attention to that subset of the SM NNLO diagrams which corresponds to EFT terms containing an extra factor $\delta^{3/2}$ with respect to the LO result, rather than δ^2 . Corrections of the same order in the EFT power counting that are already included in the SM LO or NLO diagrams (non-resonant contributions encoded in four-electron operators in the EFT; higher dimensional production operators; etc.) are not considered in the present paper. Those $N^{3/2} \text{LO}^{\text{EFT}}$ radiative corrections that correspond to SM NNLO diagrams can be readily organised in several classes:

Mixed hard/Coulomb corrections: This class is given by diagrams with a single-Coulomb photon and one insertion of a hard NLO correction to the

- *production stage:* Here the LO operator (6) is replaced by the NLO expression (figure 2a). A representative diagram of the full-SM counterpart is shown in figure 2d; this correction is computed in section 3.3.
- *decay stage:* A sample diagram in the standard loop expansion is shown in figure 2e. The implementation of this correction in the EFT discussed in section 3.7 is denoted by the black dot labelled δ_{decay} in figure 2b.
- *propagation stage:* A sample diagram in the standard loop expansion is shown in figure 2f. The implementation of this correction in the EFT discussed in section 3.8 is denoted by the black dot labelled δ_{residue} in figure 2b.

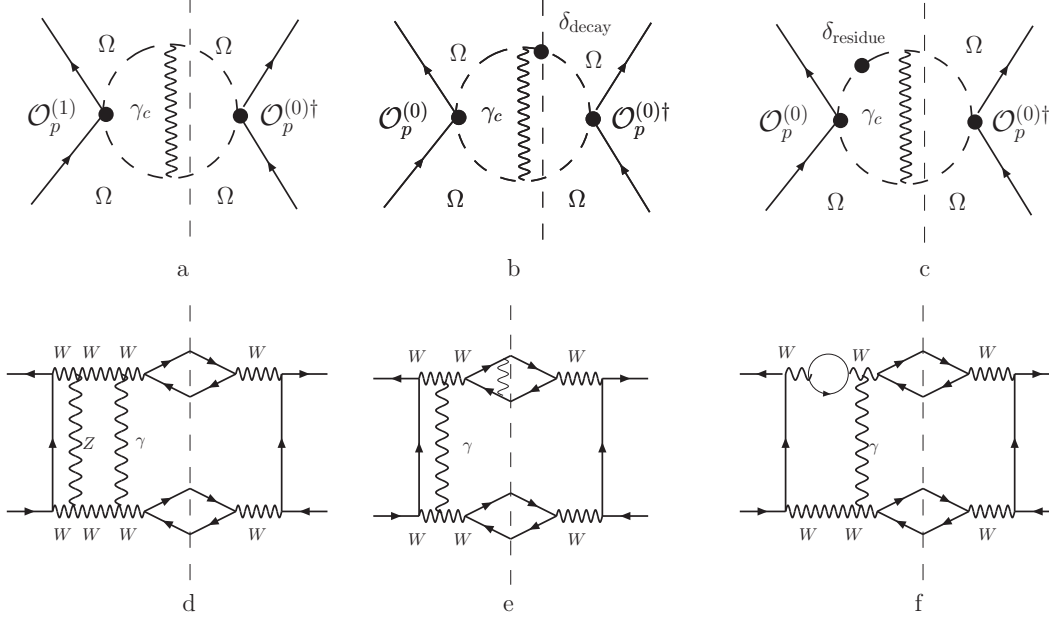


Figure 2: Sample $N^{3/2}LO^{EFT}$ diagrams in the EFT (first line) with mixed hard/Coulomb corrections and corresponding NNLO diagrams in the full SM (second line). Note the insertion of a NLO production operator in diagram a. The same conventions of figure 1 are adopted.

Interference of Coulomb and radiative corrections: There are two contributions in this class:

- *Single-Coulomb exchange and soft photons.* An EFT diagram in this class is shown in figure 3a. A representative diagram of the full-SM counterpart is shown in figure 3d. This correction is computed in section 3.2.
- *Single-Coulomb exchange and collinear photons.* These corrections (see figure 3b for a representative diagram in the EFT, and figure 3e for a counterpart in the full SM) vanish if the electron mass is set to zero. If a finite electron mass is used as infrared (IR) regulator there are further contributions from soft-collinear and hard-collinear modes that are computed in sections 3.2 and 3.3, respectively.

NLO corrections to the Coulomb potential: The relevant diagram is given by a semi-soft fermion bubble insertion into the Coulomb photon (see figure 3c for the EFT diagram and figure 3f for the counterpart in the full SM). This correction is computed in section 3.6 and appendix A.

This concludes our survey of the dominant NNLO corrections. In the next section we will compute the different contributions identified above. At the same order in the EFT power counting as the above contributions we also encounter triple-Coulomb exchange that is a NNNLO correction in the standard loop expansion. This effect can be straightforwardly included using EFT methods but turns out to be numerically negligible.

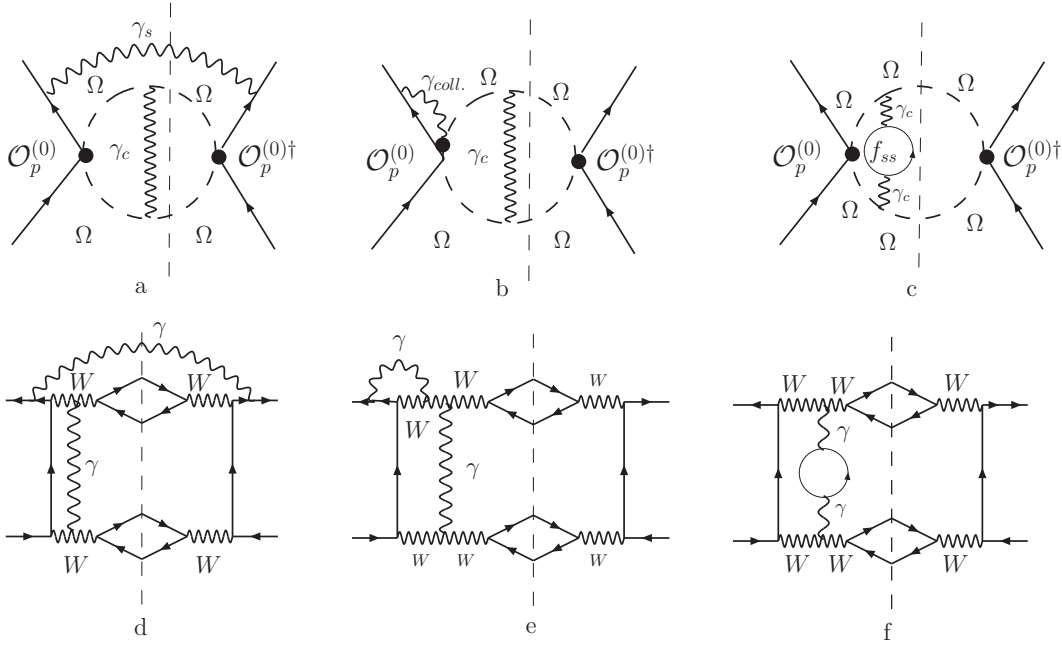


Figure 3: Sample $N^{3/2}\text{LO}^{\text{EFT}}$ diagrams with single-Coulomb exchange and radiative corrections in the EFT (first line) and corresponding NNLO diagrams in the full SM (second line). The same conventions of figure 1 are adopted.

3 Evaluation of the dominant NNLO corrections

In section 2 the dominant NNLO corrections to four-fermion production near the W -pair production threshold have been identified. In this section we compute all the relevant contributions. Subsection 3.1 reviews the known result for the all-order Coulomb Green function that will enter subsequent calculations and extracts the triple-Coulomb exchange correction. Interference of single-Coulomb exchange with corrections from soft and soft-collinear photons are computed in subsection 3.2. Subsection 3.3 contains the results for interference of single-Coulomb exchange with hard corrections to the production stage and with hard-collinear photon exchange. These computations are carried out in a form that allows in principle to include all-order Coulomb exchange as well. This subset of NNLO corrections is combined to a finite partial result in subsection 3.4 and large logarithms of the electron mass are absorbed in electron structure functions in subsection 3.5. Radiative corrections to the single-Coulomb exchange potential itself are discussed in subsection 3.6. Interference effects of single-Coulomb exchange with corrections to the decay and propagation stages are subject of subsections 3.7 and 3.8.

3.1 Coulomb Green function and triple-Coulomb exchange

It is clear that Coulomb corrections will play a privileged role in our computation. In particular, in the following, we will derive a result which can be applied to diagrams involving an arbitrary number of Coulomb photons. Therefore, in order to illustrate our formalism, we review here the computation of pure Coulomb corrections to the four-fermion production process (1), given by

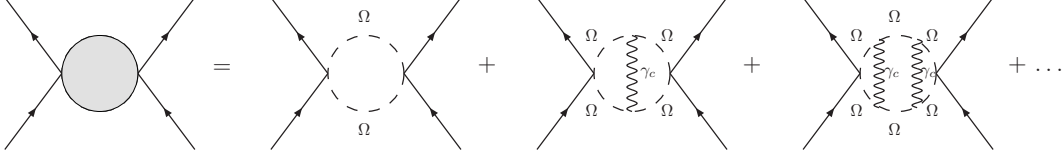


Figure 4: Pure Coulomb corrections to the forward-scattering amplitude.

the exchange of potential photons with energy $k_0 \sim M_W \delta$ and three-momentum $|\vec{k}| \sim M_W \sqrt{\delta}$. Note that these corrections correspond to insertions of non-local four-boson interactions in the effective Lagrangian of potential non-relativistic QED [20]. They can be summed to all orders in perturbation theory, as shown in figure 4, in terms of the zero-distance Coulomb Green function, the Green function $G_C^{(0)}(\vec{r}_1, \vec{r}_2; E)$ of the Schrödinger operator $-\vec{\nabla}^2/M_W - \alpha/r$ evaluated at $\vec{r}_1 = \vec{r}_2 = 0$.

Using the representation of the Green function given in [21] and defining $E \equiv \sqrt{s} - 2M_W$ and $\mathcal{E}_W \equiv E + i\Gamma_W$, we can represent the Coulomb-corrected e^-e^+ forward-scattering amplitude corresponding to the diagrams in figure 4 as

$$\mathcal{A}_{LR}^C = \frac{\pi^2 \alpha_{ew}^2}{M_W^4} \langle p_2 - |n^{[i} \gamma^{j]} | p_1 - \rangle \langle p_1 - | n^{[i} \gamma^{j]} | p_2 - \rangle G_C^{(0)}(0, 0; \mathcal{E}_W), \quad (8)$$

where we have adopted the canonical helicity notation $|p\pm\rangle \equiv \frac{1\pm\gamma^5}{2}u(p)$. The $\overline{\text{MS}}$ -subtracted representation for the zero-distance Coulomb Green function with a complex argument \mathcal{E}_W , including all-order photon exchange, reads as follows [22]:

$$G_C^{(0)}(0, 0; \mathcal{E}_W) = -\frac{M_W^2}{4\pi} \left\{ \sqrt{-\frac{\mathcal{E}_W}{M_W}} + \alpha \left[\frac{1}{2} \ln \left(-\frac{4M_W \mathcal{E}_W}{\mu^2} \right) - \frac{1}{2} + \gamma_E + \psi \left(1 - \frac{\alpha}{2\sqrt{-\mathcal{E}_W/M_W}} \right) \right] \right\}. \quad (9)$$

Here γ_E is the Euler-Mascheroni constant, μ the 't Hooft unit of mass, and ψ the Euler psi-function. The total cross section for the left-right helicity configuration can be obtained by evaluating the spinor product $\langle p_2 - | n^{[i} \gamma^{j]} | p_1 - \rangle \langle p_1 - | n^{[i} \gamma^{j]} | p_2 - \rangle = 16(1 - \epsilon) M_W^2$ and by multiplying the imaginary part of the forward-scattering amplitude (8) by the LO branching-fraction product $\text{Br}_{W^- \rightarrow \mu^- \bar{\nu}_\mu}^{(0)} \text{Br}_{W^+ \rightarrow u \bar{d}}^{(0)} = 1/27$. Finally, expanding the psi function appearing in (9) in α , we get the one- and two-Coulomb photon exchange terms [23, 24]

$$\sigma_{LR}^C = -\frac{4\pi \alpha_{ew}^2}{27 s} \text{Im} \left[\sqrt{-\frac{\mathcal{E}_W}{M_W}} + \frac{\alpha}{2} \ln \left(-\frac{\mathcal{E}_W}{M_W} \right) - \frac{\alpha^2 \pi^2}{12} \sqrt{-\frac{M_W}{\mathcal{E}_W}} \right], \quad (10)$$

where the scheme-dependent real constant of (9) has dropped out. These three terms, shown in figure 4, are already included in the NLO EFT computation.

Triple-Coulomb exchange arises from a NNNLO correction in the standard loop counting, but contributes at order $N^{3/2}\text{LO}$ in the EFT power-counting. The result can be obtained straightforwardly by expanding (9) up to order α^3 :

$$\Delta \sigma_{LR}^{C3} = \frac{\pi \alpha_{ew}^2}{27 s} \alpha^3 \zeta(3) \text{Im} \left[-\frac{M_W}{\mathcal{E}_W} \right]. \quad (11)$$

The correction to the helicity-averaged cross section $\Delta\sigma^{C3} = \Delta\sigma_{LR}^{C3}/4$ directly at threshold is $\Delta\sigma^{C3}(\sqrt{s} = 161\text{GeV}) = 0.01\text{fb}$ while the effect is even smaller away from threshold.

3.2 Soft and soft-collinear corrections

We consider here the radiative corrections obtained including soft-photon exchange to the diagrams shown in figure 4. These $\mathcal{O}(\alpha)$ contributions to the Coulomb-corrected forward-scattering amplitude are related to the initial-initial state interference diagrams in the effective theory shown in figure 5, where the photon energy and three-momentum scale both as $k_0 \sim |\vec{k}| \sim M_W \delta$. Analogously to the NLO calculation in [13], diagrams with a coupling of soft photons to Ω lines cancel as can be shown using a gauge-invariance argument. The coupling of soft photons to collinear electrons and positrons is given by the soft-collinear effective-theory (SCET) Lagrangian [25, 26, 27], and amounts to the eikonal coupling $\pm ien^\mu$, where n^μ stands for the direction of the four-momentum of the electron or the positron.

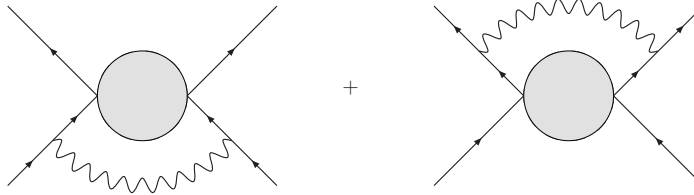


Figure 5: Soft-photon corrections to the all-order Coulomb-corrected forward-scattering amplitude.

The sum of the two diagrams shown in figure 5 can be written in close analogy with (8) as

$$i\mathcal{A}_{LR}^{C \times S} = \frac{16\pi^2 \alpha_{ew}^2}{M_W^2} (1 - \epsilon) 2\mathcal{I}_S, \quad (12)$$

where \mathcal{I}_S denotes the convolution of the zero-distance Green function and a single soft-photon exchange correction. Including prefactors it reads

$$\mathcal{I}_S \equiv -32\pi\alpha M_W^2 \tilde{\mu}^{2\epsilon} \int \frac{d^d k}{(2\pi)^d} \frac{G_C^{(0)}(0, 0; \mathcal{E}_W - k^0)}{(k^2 + i0)(-2p_1 \cdot k + i0)(-2p_2 \cdot k + i0)}. \quad (13)$$

Here the space-time dimension is $d \equiv 4 - 2\epsilon$, $\tilde{\mu}^2 \equiv \mu^2 e^{\gamma_E}/(4\pi)$ and $G_C^{(0)}$ is given, to all orders in α but in $d = 4$, in (9).

The soft integral (13) can be evaluated in two steps: first, we approximate the momenta of the external electron and positron introducing $p_1 \equiv M_W n_+$ and $p_2 \equiv M_W n_-$, where n_+ and n_- fulfil the relations $n_+^2 = n_-^2 = 0$ and $n_+ \cdot n_- = 2$; next, we perform the k^0 integration closing the integration contour in the lower complex k^0 half-plane, using Cauchy theorem and Jordan lemma and picking up the residue of the pole at $k^0 = |\vec{k}| - i0$. Note that all singularities of $G_C^{(0)}$ are located in the upper k^0 half plane. The result is

$$\mathcal{I}_S = -i \left(\frac{\alpha}{\pi} \right) \frac{\sqrt{\pi}}{\epsilon \Gamma(1/2 - \epsilon)} (e^{\gamma_E} \mu^2)^\epsilon \int_0^\infty dk \frac{G_C^{(0)}(0, 0; \mathcal{E}_W - k)}{k^{1+2\epsilon}}. \quad (14)$$

The single pole in the ϵ plane in the prefactor of (14) is associated with the emission of photons collinear to the incoming electron or positron, whose mass must be neglected in the soft region. The finite electron mass requires the introduction of two further regions (soft- and hard-collinear) [13], which convert the collinear $1/\epsilon$ pole into a large logarithm containing the electron mass. The soft-collinear correction to the forward-scattering amplitude is

$$i\mathcal{A}_{LR}^{C \times SC} = \frac{16\pi^2 \alpha_{ew}^2}{M_W^2} (1 - \epsilon) 4 \mathcal{I}_{SC}, \quad (15)$$

where the integral \mathcal{I}_{SC} , denoting the convolution of the zero-distance Green function with soft-collinear emission, is the same expression as (13), but cannot be evaluated employing the same approximations as for the soft corrections. For soft-collinear emission along the electron direction, the photon momentum satisfies $n_- \cdot k \sim \Gamma_W$, $n_+ \cdot k \sim \Gamma_W \cdot (m_e/M_W)^2$ and $k_\perp \sim m_e \Gamma_W/M_W$ with opposite-pointing light-like vectors n_\mp . In this case, we parametrise the external momenta according to $p_1 \equiv \alpha n_+ + \beta n_-$ and $p_2 \equiv \alpha n_- + \beta n_+$, and fix α and β in terms of the kinematical variables s and m_e^2 through the relations $s = 4(\alpha + \beta)^2$ and $m_e^2 = 4\alpha\beta$. The result for the soft-collinear configuration reads

$$\mathcal{I}_{SC} = \frac{i}{2} \left(\frac{\alpha}{\pi} \right) \Gamma(\epsilon) \left(\frac{M_W}{m_e} \right)^{2\epsilon} (e^{\gamma_E} \mu^2)^\epsilon \int_0^\infty dk \frac{G_C^{(0)}(0, 0; \mathcal{E}_W - k)}{k^{1+2\epsilon}}. \quad (16)$$

Summing up the soft and soft-collinear corrections (12) and (15) and using the explicit results for the integrals \mathcal{I}_S and \mathcal{I}_{SC} (14) and (16), we obtain

$$\begin{aligned} \mathcal{A}_{LR}^{C \times [S+SC]} &\equiv \mathcal{A}_{LR}^{C \times S} + \mathcal{A}_{LR}^{C \times SC} = \frac{32\pi \alpha_{ew}^2 \alpha}{M_W^2} (1 - \epsilon) \left[-\frac{\sqrt{\pi}}{\epsilon \Gamma(1/2 - \epsilon)} + \Gamma(\epsilon) \left(\frac{M_W}{m_e} \right)^{2\epsilon} \right] \times \\ &\times (e^{\gamma_E} \mu^2)^\epsilon \int_0^\infty dk \frac{G_C^{(0)}(0, 0; \mathcal{E}_W - k)}{k^{1+2\epsilon}}. \end{aligned} \quad (17)$$

As expected, the ϵ pole cancels in the prefactor of (17); the infrared sensitivity of the result is reflected in the large logarithms $\ln(M_W/m_e)$.

3.3 Production-vertex and hard-collinear corrections

We turn now to the radiative corrections to the total cross section of (1) obtained replacing the LO production operator (6) with the NLO expression

$$\mathcal{O}_p^{(1)} = \frac{\pi \alpha_{ew}}{M_W^2} \left[C_{p,LR}^{(1)} \left(\bar{e}_L \gamma^{[i} n^j] e_L \right) + C_{p,RL}^{(1)} \left(\bar{e}_R \gamma^{[i} n^j] e_R \right) \right] \left(\Omega_-^{\dagger i} \Omega_+^{\dagger j} \right). \quad (18)$$

Here the short-distance one-loop coefficients $C_{p,LR}^{(1)}$ and $C_{p,RL}^{(1)}$ follow from the matching procedure introduced in [15, 28]: first, the one-loop $e_{L/R}^- e_{R/L}^+ \rightarrow W^- W^+$ scattering amplitude is computed at LO in the non-relativistic approximation; next, the result is matched with the amplitude obtained with the tree-level operator in the effective theory. For our purposes, the one-loop coefficient $C_{p,RL}^{(1)}$ is irrelevant, since the $e_R^- e_L^+$ helicity configuration does not give

any LO contribution, and no interference between the RL and LR configurations arises. As explained in [13] we need to take into account only the real part of $C_{p,LR}^{(1)}$,

$$\text{Re } C_{p,LR}^{(1)} = \frac{\alpha}{2\pi} \text{Re} \left[\left(-\frac{1}{\epsilon^2} - \frac{3}{2\epsilon} \right) \left(-\frac{4M_W^2}{\mu^2} \right)^{-\epsilon} + c_{p,LR}^{(1,\text{fin})} \right]. \quad (19)$$

The finite part $c_{p,LR}^{(1,\text{fin})}$ is given explicitly in Appendix B.1 of [13]; numerically, we have $\text{Re } c_{p,LR}^{(1,\text{fin})} = -10.076$ for $M_W = 80.377$ GeV, $M_Z = 91.188$ GeV, top-quark mass $m_t = 174.2$ GeV and Higgs mass $M_H = 115$ GeV. The hard production-vertex contributions to the Coulomb-corrected forward-scattering amplitude can be readily obtained appending twice the one-loop coefficient (19) to the expression in (8),

$$\text{Im } \mathcal{A}_{LR}^{\text{C}\times\text{H}} = \frac{16\pi^2 \alpha_{ew}^2}{M_W^2} (1-\epsilon) 2 \text{Re } C_{p,LR}^{(1)} \text{Im } G_C^{(0)}(0,0;\mathcal{E}_W). \quad (20)$$

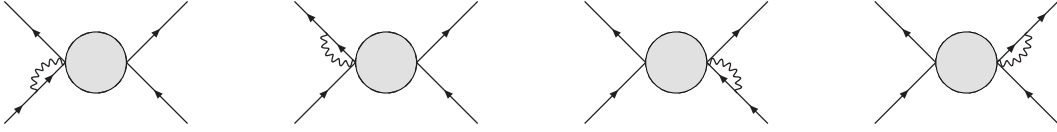


Figure 6: Hard-collinear photon corrections to the all-order Coulomb-corrected forward-scattering amplitude.

Finally, we consider the hard-collinear photon corrections illustrated in figure 6, associated with momentum scalings $k^0 \sim M_W$ and $k^2 \sim m_e^2$. The collinear-photon couplings arise from the SCET Lagrangian, and their couplings to the W bosons are encoded in collinear Wilson lines $W_{c_{1/2}}$ incorporated in the production operators by replacing the electron field $e_{c_1,L}$ by $W_{c_1}^\dagger e_{c_1,L}$ and analogously for the positron field $\bar{e}_{c_2,L}$. Hard-collinear photon corrections to the forward-scattering amplitude clearly have a factorised form; their contribution can be obtained multiplying (8) by the hard-collinear factor derived in [13],

$$\begin{aligned} \mathcal{A}_{LR}^{\text{C}\times\text{HC}} &= \frac{16\pi^2 \alpha_{ew}^2}{M_W^2} (1-\epsilon) G_C^{(0)}(0,0;\mathcal{E}_W) \times \\ &\times \frac{\alpha}{\pi} \left\{ \frac{1}{\epsilon^2} + \frac{1}{\epsilon} \left[-2 \ln \left(\frac{m_e}{\mu} \right) + \frac{3}{2} \right] + 2 \ln^2 \left(\frac{m_e}{\mu} \right) - 3 \ln \left(\frac{m_e}{\mu} \right) + \frac{\pi^2}{12} + 3 \right\}. \end{aligned} \quad (21)$$

Summing up the production-vertex and hard-collinear photon corrections (20) and (21) we obtain

$$\begin{aligned} \text{Im } \mathcal{A}_{LR}^{\text{C}\times[\text{H}+\text{HC}]} &\equiv \text{Im} \left(\mathcal{A}_{LR}^{\text{C}\times\text{H}} + \mathcal{A}_{LR}^{\text{C}\times\text{HC}} \right) = \frac{16\pi \alpha_{ew}^2 \alpha}{M_W^2} (1-\epsilon) \text{Im } G_C^{(0)}(0,0;\mathcal{E}_W) \times \\ &\times \left\{ 2 \ln \left(\frac{2M_W}{m_e} \right) \left[\frac{1}{\epsilon} + \ln \left(\frac{2M_W}{m_e} \right) - \ln \left(\frac{4M_W^2}{\mu^2} \right) + \frac{3}{2} \right] + 3 + \frac{7\pi^2}{12} + \text{Re } c_{p,LR}^{(1,\text{fin})} \right\}. \end{aligned} \quad (22)$$

3.4 The total cross section

The combination of (17) and (22) represents our basic expression for the higher order contributions to the all-order Coulomb-corrected forward-scattering $e_L^- e_R^+$ amplitude in the effective theory. In order to better exploit the structure of the result and show how the cancellation of poles in the ϵ plane takes place, we introduce a modified ‘+’ distribution,

$$\int_0^\infty dk \frac{f(k)}{[k]_{a+}} \equiv \int_0^a dk \frac{f(k) - f(0)}{k} + \int_a^\infty dk \frac{f(k)}{k}, \quad (23)$$

where a is an arbitrary positive real parameter. This parametrisation allows us to cast the integral containing the zero-distance Coulomb Green function on the right-hand side of (17) into

$$\mu^{2\epsilon} \int_0^\infty dk \frac{f(k)}{k^{1+2\epsilon}} = \left[-\frac{1}{2\epsilon} + \ln\left(\frac{a}{\mu}\right) \right] f(0) + \int_0^\infty dk \frac{f(k)}{[k]_{a+}} + \mathcal{O}(\epsilon), \quad (24)$$

with $f(k) \equiv G_C^{(0)}(0, 0; \mathcal{E}_W - k)$; therefore we can prove explicitly that the sum of (17) and (22) is free from ϵ poles. The full correction to the total cross section (1) reads

$$\begin{aligned} \frac{\sigma_{LR}^{C \times [S+H]}}{27s} &\equiv \frac{1}{27s} \text{Im} \left(\mathcal{A}_{LR}^{C \times [S+SC]} + \mathcal{A}_{LR}^{C \times [H+HC]} \right) \\ &= \frac{16\pi \alpha_{ew}^2 \alpha}{27s M_W^2} \left\{ 4 \ln\left(\frac{2M_W}{m_e}\right) \text{Im} \int_0^\infty dk \frac{G_C^{(0)}(0, 0; \mathcal{E}_W - k)}{[k]_{a+}} \right. \\ &\quad \left. + \left[\left(3 - 4 \ln\left(\frac{M_W}{a}\right) \right) \ln\left(\frac{2M_W}{m_e}\right) + 3 + \frac{\pi^2}{4} + \text{Re} c_{p,LR}^{(1,\text{fin})} \right] \text{Im} G_C^{(0)}(0, 0; \mathcal{E}_W) \right\}. \end{aligned} \quad (25)$$

Now, after all poles in ϵ have cancelled, $G_C^{(0)}(0, 0; \mathcal{E}_W)$ can be taken to be the four-dimensional expression given in (9). The result of [13] for the NLO correction to the total cross section at the partonic level can be readily re-derived inserting the zero-Coulomb exchange term of (9) into (25), and observing that

$$\text{Im} \int_0^\infty dk \frac{1}{[k]_{a+}} \sqrt{-\frac{\mathcal{E}_W - k}{M_W}} = \text{Im} \left\{ \sqrt{-\frac{\mathcal{E}_W}{M_W}} \left[\ln\left(-\frac{4\mathcal{E}_W}{a}\right) - 2 \right] \right\}. \quad (26)$$

The new $N^{3/2}\text{LO}^{\text{EFT}}$ correction follows from inserting the one-Coulomb exchange term of (9) into (25) for the total cross section; after performing explicitly the k integration,

$$\text{Im} \int_0^\infty dk \frac{1}{[k]_{a+}} \ln\left(-\frac{4M_W(\mathcal{E}_W - k)}{\mu^2}\right) = \text{Im} \left[\frac{1}{2} \ln^2\left(-\frac{\mathcal{E}_W}{M_W}\right) - \ln\left(-\frac{\mathcal{E}_W}{M_W}\right) \ln\left(\frac{a}{M_W}\right) \right], \quad (27)$$

we get

$$\begin{aligned} \Delta \bar{\sigma}_{LR}^{C \times [S+H]} &= \frac{4\alpha_{ew}^2 \alpha^2}{27s} \text{Im} \left\{ -\frac{1}{2} \ln\left(-\frac{\mathcal{E}_W}{M_W}\right) \left[2 \ln\left(-\frac{\mathcal{E}_W}{M_W}\right) \ln\left(\frac{2M_W}{m_e}\right) \right. \right. \\ &\quad \left. \left. + 3 \ln\left(\frac{2M_W}{m_e}\right) + 3 + \frac{\pi^2}{4} + \text{Re} c_{p,LR}^{(1,\text{fin})} \right] \right\}. \end{aligned} \quad (28)$$

The dependence on the a regulator has obviously cancelled; the result is finite in the ϵ plane, but the infrared sensitivity of the cross section is reflected in the large logarithms $\ln(2M_W/m_e)$. In the next section we show how to absorb the large logarithms in the electron distribution function.

3.5 Initial-state radiation

An accurate prediction for the total cross section of (1) requires to resum the collinear logarithms from initial-state radiation (ISR). Here we apply the strategy outlined in [13], employing the electron structure function Γ_{ee}^{LL} provided in [29, 30]. The ISR resummed cross section for a given helicity configuration h is

$$\sigma_h(s) \equiv \int_0^1 dx_1 \int_0^1 dx_2 \Gamma_{ee}^{\text{LL}}(x_1) \Gamma_{ee}^{\text{LL}}(x_2) \hat{\sigma}_h(x_1 x_2 s), \quad (29)$$

where the partonic cross section $\hat{\sigma}_h$ denotes the sum of the Born result and the higher-order correction, $\hat{\sigma}_h = \sigma_h^{\text{Born}} + \hat{\sigma}_h^{\text{h.o.}}$, with logarithms of the electron mass subtracted such that expansion of (29) reproduces the NLO cross section.

Therefore, we construct $\Delta \hat{\sigma}_{LR}^{\text{C} \times [\text{S}+\text{H}]}$ starting from $\Delta \bar{\sigma}_{LR}^{\text{C} \times [\text{S}+\text{H}]}$ of (25) and performing a subtraction,

$$\Delta \hat{\sigma}_{LR}^{\text{C} \times [\text{S}+\text{H}]}(s) \equiv \Delta \bar{\sigma}_{LR}^{\text{C} \times [\text{S}+\text{H}]}(s) - 2 \int_0^1 dx \Gamma_{ee}^{\text{LL},(1)}(x) \sigma_{LR}^{\text{C}}(xs), \quad (30)$$

where $\Gamma_{ee}^{\text{LL},(1)}$ is the $\mathcal{O}(\alpha)$ term in the expansion of the conventional structure function provided in [29, 30], evaluated at $\sqrt{s} = 2M_W$, and σ_{LR}^{C} is related to the all-order Coulomb-corrected forward-scattering amplitude (8) through the usual relation $\sigma_{LR}^{\text{C}} = \text{Im} \mathcal{A}_{LR}^{\text{C}} / (27s)$. Note that the zero-distance Coulomb Green function appearing in (8) has now to be evaluated with the replacement $E \rightarrow E - M_W(1-x)$. Using $\Gamma_{ee}^{\text{LL},(1)}$ in the limit $x \rightarrow 1$,

$$\Gamma_{ee}^{\text{LL},(1)}(x) \rightarrow \frac{\alpha}{2\pi} \left[2 \ln \left(\frac{2M_W}{m_e} \right) - 1 \right] \left\{ \frac{2}{[1-x]_+} + \frac{3}{2} \delta(1-x) \right\}, \quad (31)$$

we can write the subtraction term appearing in (30) as

$$\begin{aligned} -2 \int_0^1 dx \Gamma_{ee}^{\text{LL},(1)}(x) \sigma_{LR}^{\text{C}}(xs) &= -\frac{16\pi\alpha_{ew}^2\alpha}{27sM_W^2} \left[2 \ln \left(\frac{2M_W}{m_e} \right) - 1 \right] \times \\ &\times \text{Im} \left\{ \frac{3}{2} G_{\text{C}}^{(0)}(0, 0; \mathcal{E}_W) + 2 \int_0^\infty dk \frac{G_{\text{C}}^{(0)}(0, 0; \mathcal{E}_W - k)}{[k]_{M_W+}} \right\}. \end{aligned} \quad (32)$$

To obtain this result, a term involving the integral $\text{Im}[\int_{M_W}^\infty dk G_{\text{C}}^{(0)}(0, 0; \mathcal{E}_W - k)/k]$, which is suppressed by a power of \mathcal{E}_W/M_W and corresponds to hard-collinear initial-state radiation, has been dropped. Replacing (32) and (25) in (30) and choosing $a = M_W$, we finally obtain

$$\hat{\sigma}_{LR}^{\text{C}}(s) = \frac{16\pi\alpha_{ew}^2\alpha}{27sM_W^2} \left[\left(\frac{9}{2} + \frac{\pi^2}{4} + \text{Re} c_{p,LR}^{(1),\text{fin}} \right) \text{Im} G_{\text{C}}^{(0)}(0, 0; \mathcal{E}_W) + 2 \text{Im} \int_0^\infty dk \frac{G_{\text{C}}^{(0)}(0, 0; \mathcal{E}_W - k)}{[k]_{M_W+}} \right], \quad (33)$$

where the dependence on the large logarithms $\ln(2M_W/m_e)$ has cancelled out.

Using (27) for the one-Coulomb exchange term in (9), we get the $\text{N}^{3/2}\text{LO}^{\text{EFT}}$ contribution to the total cross section to be convoluted with the electron structure functions in (29),

$$\Delta \hat{\sigma}_{LR}^{\text{C} \times [\text{S}+\text{H}]} = -\frac{\alpha_{ew}^2\alpha^2}{27s} \left\{ \left(9 + \frac{\pi^2}{2} + 2 \text{Re} c_{p,LR}^{(1),\text{fin}} \right) \text{Im} \left[\ln \left(-\frac{\mathcal{E}_W}{M_W} \right) \right] + 2 \text{Im} \left[\ln^2 \left(-\frac{\mathcal{E}_W}{M_W} \right) \right] \right\}. \quad (34)$$

The result has been cross-checked through a direct integration of the one-Coulomb exchange terms.

3.6 Corrections to the Coulomb potential

$N^{3/2}\text{LO}^{\text{EFT}}$ contributions also arise from semi-soft and hard corrections to the Coulomb force between the two W s. The hard corrections are closely related to the renormalisation of the electromagnetic coupling in the Coulomb potential; they are discussed in detail in appendix A.

As a first example for semi-soft modes, consider corrections from light fermions that consist of the insertion of a fermion bubble into a photon propagator exchanged between two W -lines as shown in figure 7a but also vertex corrections (figure 7b) and box corrections (figure 7c). For a potential photon the only correction at order $N^{3/2}\text{LO}$ comes from the bubble insertion where the fermion is semi-soft, leading to the effective theory diagram shown in figure 7d. Since the semi-soft fermion propagator $1/k_{ss}$ counts as $\delta^{-1/2}$ and the loop measure as $d^4k_{ss} \sim \delta^2$ the fermion loop insertion scales as $\alpha\delta^1 \sim \delta^2$. Taking the additional potential photon propagator $\sim \delta^{-1}$ into account this diagram is suppressed by a factor δ compared to the pure single-Coulomb exchange and is therefore a $N^{3/2}\text{LO}$ correction to the forward-scattering amplitude. The triangle diagrams and box diagrams with semi-soft fermions do not contribute at order $N^{3/2}\text{LO}$ as can be seen from a power-counting argument. For instance, in the triangle diagram of figure 7b the semi-soft loop momentum can be neglected compared to the W -mass so the neutrino propagator contains no momentum dependence. By the same arguments as before the diagram is of order δ^2 compared to the single-Coulomb exchange and does not have to be considered.

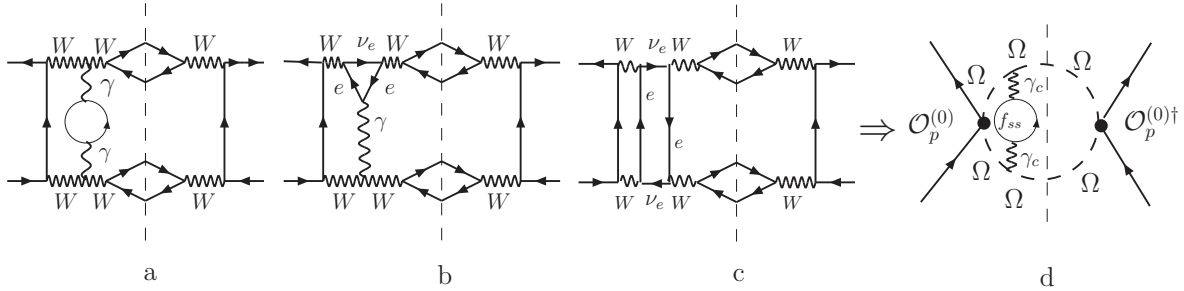


Figure 7: a-c: Sample diagrams in the full SM that potentially give rise to corrections from semi-soft fermions. Only the insertion of a semi-soft fermion bubble (a) contributes at $N^{3/2}\text{LO}$ and leads to the EFT diagram shown in d.

Another $N^{3/2}\text{LO}$ correction potentially arises from box diagrams with exchange of two semi-soft photons. Example diagrams in the full theory are shown in figure 8a-c, and a representative diagram in the effective theory is shown in figure 8d. After interacting with a semi-soft photon with momentum k_{ss} , the W propagator turns into $1/(2M_W k_{ss,0}) \sim \delta^{-1/2}$. Note that $k_{ss,0} \sim M_W \sqrt{\delta} \gg \Gamma_W$ so that the decay width can be treated perturbatively in the semi-soft region. Since the photon propagators are given by $1/k_{ss}^2 \sim \delta^{-1}$, the semi-soft subgraph counts as $\alpha^2 d^4k_{ss} (1/k_{ss}^2)^2 1/(2k_{ss,0})^2 \sim \alpha^2 \delta^{-1}$. The potential sub-loop of the box diagram figure 8d has two Ω propagators so it scales as $\delta^{5/2} \delta^{-2}$. Therefore the contribution of these diagrams would again be suppressed by $\delta^{3/2}$ compared to the leading order. However, at leading order in the non-relativistic expansion the diagrams shown in figure 8a and 8b cancel each other. For this it is essential that the width in the propagator can be treated perturbatively in the semi-soft region and is not resummed in the propagator. Diagrams that contain a quartic vertex

like 8c contribute only at higher orders because they miss at least one factor $1/k_{ss,0}$ from a W -propagator compared to figure 8a/b. Therefore there are no contributions from semi-soft photons at the order we consider here. In QED this is well known from explicit calculations of the Coulomb potential [32, 33].

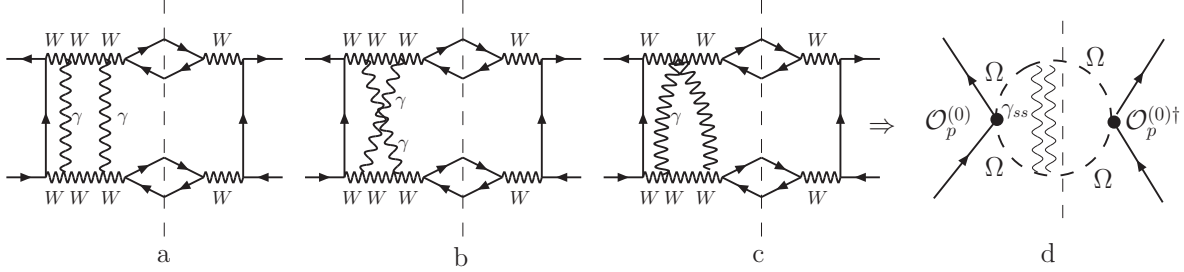


Figure 8: a-c: Sample diagrams in the full SM that potentially give rise to corrections from semi-soft photons. A sample diagram in the EFT is shown in d. As discussed in the text these diagrams do not contribute at $N^{3/2}\text{LO}$.

The only corrections to be calculated are therefore the semi-soft fermion bubble insertion in the single-Coulomb exchange diagram shown in figure 7d and the hard corrections discussed in appendix A. For convenience we will perform the calculation in the $\alpha(M_Z)$ scheme (see e.g. [31, 34]) and convert the result afterwards to the G_μ scheme used in [13]. The hard corrections to the forward-scattering amplitude are proportional to the single Coulomb exchange, hence

$$\Delta\mathcal{A}_{LR}^{\text{NLO-C}}|_{\alpha(M_Z)} = \Delta\mathcal{A}_{LR}^{\text{ss}} + \mathcal{A}_{LR}^{\text{C1}} \delta_{\text{hard}}^{\alpha(M_Z)}, \quad (35)$$

where $\Delta\mathcal{A}_{LR}^{\text{ss}}$ is the unrenormalised semi-soft amplitude shown in figure 7d, and $\mathcal{A}_{LR}^{\text{C1}}$ the single-Coulomb correction to the forward-scattering amplitude included in (8). The hard correction is given in (67) and involves the contribution of the light fermions (leptons and quarks except top) to the vacuum polarisation evaluated at M_Z :

$$\delta_{\text{hard}}^{\alpha(M_Z)} = -\frac{\text{Re} \Pi_{f \neq t}^{AA}(M_Z^2)}{M_Z^2} = \sum_f C_f Q_f^2 2 \left(\frac{\alpha}{\pi} \right) e^{\gamma_E \epsilon} \Gamma(\epsilon) \text{Re} \left[\left(-\frac{M_Z^2}{\mu^2} \right)^{-\epsilon} \right] \frac{\Gamma^2(2-\epsilon)}{\Gamma(4-2\epsilon)}. \quad (36)$$

Here $C_f = 1$ for the leptons and $C_f = N_c = 3$ for the quarks, and Q_f is the electric charge of f in units of e , such that $\sum_f C_f Q_f^2 = 20/3$. The total correction to the forward-scattering amplitude from the semi-soft bubble and the hard correction, at all orders in ϵ , is given by

$$\begin{aligned} \Delta\mathcal{A}_{LR}^{\text{NLO-C}}|_{\alpha(M_Z)} = & - \sum_f C_f Q_f^2 \frac{\alpha_{ew}^2 \alpha^2}{2\pi} e^{3\gamma_E \epsilon} (1-\epsilon) \frac{1}{\epsilon} \frac{\Gamma(\epsilon) \Gamma^2(2-\epsilon)}{\Gamma(4-2\epsilon) \Gamma(3/2-\epsilon)} \times \\ & \times \left[\left(\frac{M_W}{\mu} \right)^{-3\epsilon} \left(-\frac{\mathcal{E}_W}{\mu} \right)^{-3\epsilon} \frac{\Gamma(3\epsilon) \Gamma(1/2-2\epsilon) \Gamma^2(1/2+2\epsilon)}{\Gamma(4\epsilon)} \right. \\ & \left. - 2 \left(\frac{M_W}{\mu} \right)^{-2\epsilon} \left(-\frac{\mathcal{E}_W}{\mu} \right)^{-2\epsilon} \text{Re} \left[\left(-\frac{M_Z^2}{\mu^2} \right)^{-\epsilon} \right] \Gamma(1/2-\epsilon) \Gamma^2(1/2+\epsilon) \right]. \quad (37) \end{aligned}$$

Expanding (37) in ϵ one gets

$$\Delta\sigma_{LR}^{\text{NLO-C}}|_{\alpha(M_Z)} = -\frac{\alpha_{ew}^2\alpha^2}{81s} \sum_f C_f Q_f^2 \left\{ 4\ln\left(\frac{2M_W}{M_Z}\right) \text{Im}\left[\ln\left(-\frac{\mathcal{E}_W}{M_W}\right)\right] + \text{Im}\left[\ln^2\left(-\frac{\mathcal{E}_W}{M_W}\right)\right] \right\}. \quad (38)$$

While this result is valid in the $\alpha(M_Z)$ scheme, the numerical results in [13] were given in the G_μ scheme. According to the discussion in appendix A the result (37) can be converted to the latter scheme by adding another term:

$$\begin{aligned} \Delta\sigma_{LR}^{\text{NLO-C}} &= \Delta\sigma_{LR}^{\text{NLO-C}}|_{\alpha(M_Z)} + \delta_{\alpha(M_Z) \rightarrow G_\mu} \Delta\sigma_{LR}^{\text{C1}} \\ &= \Delta\sigma_{LR}^{\text{NLO-C}}|_{\alpha(M_Z)} - \frac{2\pi\alpha_{ew}^2\alpha}{27s} \delta_{\alpha(M_Z) \rightarrow G_\mu} \text{Im}\left[\ln\left(-\frac{\mathcal{E}_W}{M_W}\right)\right], \end{aligned} \quad (39)$$

where the single-Coulomb exchange cross-section $\Delta\sigma_{LR}^{\text{C1}}$ is the order α correction in (10). The result for the finite conversion factor $\delta_{\alpha(M_Z) \rightarrow G_\mu}$ is given in (72) in appendix A. For the same input parameters as used for the hard-matching coefficient below (19) the numerical value is given by $\delta_{\alpha(M_Z) \rightarrow G_\mu} = 4.103\alpha$.

3.7 Decay corrections

In (34) the radiative corrections to the imaginary part of the forward-scattering amplitude are multiplied by the leading-order branching fraction product $\text{Br}^{(0)}(W^- \rightarrow \mu^- \bar{\nu}_\mu) \text{Br}^{(0)}(W^+ \rightarrow u\bar{d}) = 1/27$ to extract the correction to the flavour-specific four-fermion production cross section. This treatment can be shown to correspond to cutting the string of fermion bubbles implicitly contained in the resummed propagator and selecting only those cuts that contribute to the desired four-fermion final state [13]. In addition to the effects described correctly by (34) there are flavour-specific radiative corrections to the decay stage contributing at $\text{N}^{3/2}\text{LO}^{\text{EFT}}$. These arise from diagrams in the full theory such as shown in figure 2e, and the cuts corresponding to real emission from the final state.

These flavour-specific corrections are included in the EFT calculation by adding the term

$$\Delta\sigma_{LR}^{\text{C}\times\text{decay}} = \left(\frac{\Gamma_{\mu^- \bar{\nu}_\mu}^{(1,ew)}}{\Gamma_{\mu^- \bar{\nu}_\mu}^{(0)}} + \frac{\Gamma_{u\bar{d}}^{(1,ew)}}{\Gamma_{u\bar{d}}^{(0)}} \right) \Delta\sigma_{LR}^{\text{C1}}, \quad (40)$$

where the one-loop electroweak corrections to the partial decay-widths, $\Gamma_{\mu^- \bar{\nu}_\mu}^{(1,ew)}$ and $\Gamma_{u\bar{d}}^{(1,ew)}$, can be found in [13]. Note that the numerical predictions presented in [13] already include the 2-loop QCD corrections to the hadronic decay-width multiplied by the full NLO electroweak cross section (including the single-Coulomb exchange). Therefore QCD corrections do not have to be considered in this work.

3.8 Residue corrections to the W -propagators

In the proper effective-theory treatment of the computation of matching coefficients one has to include a factor $\sqrt{2M_W}(\varpi R_{hW})^{-1/2}$ for each external Ω line [13, 15]. Here ϖ accounts for the normalisation of non-relativistic fields and R_{hW} is the hard contribution to the LSZ residue of

the W propagator. Introducing an expansion of the transverse self-energy around M_W^2 and in the number of loops,

$$\Pi_T^W(k^2) = M_W^2 \sum_{m,n} \delta^n \Pi^{(m,n)}, \quad (41)$$

with $\delta = (k^2 - M_W^2)/M_W^2$ and m denoting the loop order one has to one-loop accuracy [15]

$$R_{hW}^{-1} = 1 - \Pi^{(1,1)}. \quad (42)$$

Using the on-shell scheme for field renormalisation where $\text{Re } \Pi^{(1,1)} = 0$, the residue correction is purely imaginary, $R_{hW}^{-1} = 1 - i \text{Im } \Pi^{(1,1)} = 1 + i \Gamma_W^{(0)}/M_W$ with $\Gamma_W^{(0)}$ the tree-level on-shell width. In the EFT treatment these factors reproduce the expansion of the full renormalised (transverse) W -propagator

$$P(k) = \frac{i}{k^2 - M_W^2 - \Pi_T^W(k^2)} = \frac{i}{2M_W \left(r_0 - \frac{\vec{r}^2}{2M_W} + \frac{i\Gamma_W^{(0)}}{2} \right)} \left(1 + \Pi^{(1,1)} + \varpi^{(1)} \right) + \dots, \quad (43)$$

where the NLO contribution to the non-relativistic normalisation factor, $\varpi^{(1)}$, can be found in [13], but is not needed here since in the full NLO calculation in the fixed-width or complex-mass scheme no non-relativistic expansion is performed.

At order $N^3/2$ LO the residue corrections have to be included in the single-Coulomb exchange diagram. This corresponds to including the proper factors of $\sqrt{R_{hW}}$ in the NLO matching coefficient $C_{p,LR}^{(1)}$ of the production operator in the calculation in section 3.3 and the $WW\gamma$ vertex in appendix A. In order to separate the effects corresponding to genuine loop diagrams in the standard loop expansion from those included in a tree-calculation using a fixed-width prescription, in [13] and this paper we departed from the matching procedure sketched above and did not include the factors $\varpi_{R_{hW}}$ in the computation of the hard matching coefficients. Therefore they have to be discussed separately, paying some attention to isolate those contributions that are not included in a fixed-order NLO calculation in the fixed-width or complex-mass scheme.

The factor ϖ is solely due to the use of a non-relativistic propagator. Since no kinematic expansion is performed in the calculation in the fixed-width or complex-mass scheme, all corrections of this kind are already included in [11, 12] and do not have to be considered here. This leaves the corrections from the derivative of the self-energy, $\Pi^{(1,1)}$, in (43). As shown in figure 9 these corrections contribute in two different ways to the imaginary part of the forward-scattering amplitude. In this figure we indicated the propagators of the non-relativistic W s by the abbreviations

$$\eta_r^- = r^0 - \frac{\vec{r}^2}{2M_W} + i \frac{\Gamma_W^{(0)}}{2}, \quad \eta_r^+ = E - r^0 - \frac{\vec{r}^2}{2M_W} + i \frac{\Gamma_W^{(0)}}{2}. \quad (44)$$

The cut through the propagator in figure 9a, $2 \text{Im}[1/\eta] = -\Gamma_W^{(0)}/|\eta|^2$, is interpreted as a cut through a self-energy insertion implicitly contained in the resummed propagator. To select the flavour-specific final state, the total decay width in the numerator has to be replaced by the (leading order) partial decay width $\Gamma_{\mu^-\bar{\nu}_\mu}^{(0)}$ or $\Gamma_{u\bar{d}}^{(0)}$ [13]. This diagram therefore corresponds to a single-Coulomb photon exchange diagram in the full theory with the insertion of a W self-energy, expanded to first order around the mass-shell. These contributions are not included in the fixed-order NLO calculation in the fixed-width or complex-mass scheme where only the

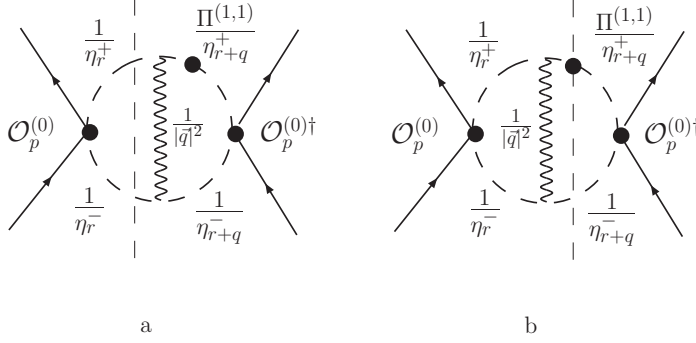


Figure 9: Cut EFT diagrams contributing to the residue corrections to the imaginary part of the forward-scattering amplitude. The Ω propagator with a dot indicates the insertion of a $\Pi^{(1,1)}$ correction factor coming from the expansion of the propagator around the pole (43). The propagators are defined in (44). Analogous diagrams with insertions at the other three Ω propagators are not shown.

self-energy evaluated at M_W^2 is resummed in the propagator [12]. In contrast the diagram in figure 9b includes a cut through a propagator modified by the factor of $\Pi^{(1,1)} = -i\Gamma_W^{(0)}/M_W$. The explicit expression is given by

$$2\text{Im}\left[\frac{\Pi^{(1,1)}}{\eta}\right] = -\frac{\Gamma_W^{(0)}}{M_W}\left(r_0 - \frac{\vec{r}^2}{2M_W}\right)\frac{1}{|\eta|^2}. \quad (45)$$

This contribution corresponds to a full-theory diagram with single-Coulomb exchange and kinematical correction from the expansion of a decay matrix element around the mass-shell. This interpretation is confirmed by inserting the one-loop result $\text{Im}\Pi_T^W(k^2) = -k^2\Gamma_W^{(0)}/M_W\theta(k^2)$ for the decay into massless fermions into the resummed propagator on the left-hand side of (43):

$$\text{Im}[-iP(k)] = \frac{-M_W\left(k^2\Gamma_W^{(0)}/M_W^2\right)}{(k^2 - M_W^2)^2 + M_W^2\left(k^2\Gamma_W^{(0)}/M_W^2\right)^2} + O(1). \quad (46)$$

A fixed-width prescription as employed in the complex-mass scheme corresponds to replacing $k^2\Gamma_W^{(0)}/M_W^2$ by $\Gamma_W^{(0)}$ in the denominator, but not in the numerator, where the factor of k^2 arises from the integration over the two-particle phase space of the W decay products. Decomposing the W -momentum as $k = M_W v + r$ with $v = (1, \vec{0})$ and a potential residual momentum r shows that the $\mathcal{O}(\delta)$ correction from expanding the factor k^2 in the numerator is indeed given by (45) (up to the usual normalisation factor $2M_W$). Since in the fixed-order calculation of four-fermion production the decays are treated without kinematical approximations, this term does not correspond to a genuine NNLO contribution and must not be included here.

The only correction that has to be included therefore are four cut diagrams of the form of figure 9a with the residue correction inserted at the different W -propagators. In the following we use again the full on-shell width Γ_W rather than the tree-expression $\Gamma_W^{(0)}$. Shifting the loop

momenta in some of the diagrams, the sum of the four terms can be brought to the form

$$\begin{aligned}\Delta\sigma_{LR}^{\text{C}\times\text{res}} &= -\frac{32(1-\epsilon)\pi^3\alpha_{ew}^2\alpha}{27M_W^2s}\tilde{\mu}^{4\epsilon}\int\frac{d^dr}{(2\pi)^d}\int\frac{d^dq}{(2\pi)^d}2\text{Im}\left[\frac{1}{\eta_r^+}\right]2\text{Im}\left[\frac{1}{\eta_r^-}\right]2\text{Re}\left[\frac{i}{\tilde{q}^2}\frac{2\Pi^{(1,1)}}{\eta_{r+q}^+\eta_{r+q}^-}\right] \\ &= -\frac{32(1-\epsilon)\pi^2\alpha_{ew}^2\Gamma_W}{27M_W^3s}\times \\ &\quad \times\left[\text{Re}G_{C1}^{(0)}(0,0,\mathcal{E}_W)-4\pi\alpha\tilde{\mu}^{4\epsilon}\int\frac{d^dr}{(2\pi)^d}\int\frac{d^dq}{(2\pi)^d}\frac{1}{\tilde{q}^2}\frac{1}{\eta_r^+\eta_r^-(\eta_{r+q}^+)^*(\eta_{r+q}^-)^*}\right].\end{aligned}\quad (47)$$

Here $G_{C1}^{(0)}$ denotes the single-Coulomb exchange term in the Coulomb Green function (9). Terms that vanish upon performing the q_0 and r_0 integrations by closing the integration contour in the upper half-plane have been dropped. The explicit computation of (47) leads to

$$\Delta\sigma_{LR}^{\text{C}\times\text{res}} = \frac{4\pi\alpha_{ew}^2\alpha}{27s}\frac{\Gamma_W}{M_W}\ln\left[\frac{2|\mathcal{E}_W|(\text{Re}\mathcal{E}_W+|\mathcal{E}_W|)}{\Gamma_W^2}\right].\quad (48)$$

4 Numerical analysis

We can now assemble the $\text{N}^{3/2}\text{LO}$ contribution to the total cross section of the scattering process $e^-e^+ \rightarrow \mu^-\bar{\nu}_\mu u\bar{d} + X$, given by the sum of the several corrections computed in section 3,

$$\hat{\sigma}_{LR}^{(3/2)} = \Delta\hat{\sigma}_{LR}^{\text{C}\times[\text{S}+\text{H}]} + \Delta\sigma_{LR}^{\text{NLO-C}} + \Delta\sigma_{LR}^{\text{C}\times\text{decay}} + \Delta\sigma_{LR}^{\text{C}\times\text{res}} + \Delta\sigma_{LR}^{\text{C}^3},\quad (49)$$

which is to be inserted into the convolution with the electron structure functions in (29). Recall that this refers to the $e_L^-e_R^+$ helicity state while there are no radiative corrections to the other helicity combinations from NNLO SM diagrams that contribute at $\text{N}^{3/2}\text{LO}$ in the EFT power counting. As input parameters for the masses of the gauge bosons and the W width we use

$$M_W = 80.377\text{ GeV}, \quad \Gamma_W = 2.09201\text{ GeV}, \quad M_Z = 91.188\text{ GeV}.\quad (50)$$

In addition, we employ for the masses of the electron, the top quark and the Higgs boson

$$m_e = 0.51099892\text{ MeV}, \quad m_t = 174.2\text{ GeV}, \quad M_H = 115\text{ GeV},\quad (51)$$

and we extract the fine-structure constant α from the relation $\alpha = \sqrt{2}G_\mu M_W^2 s_w^2/\pi$, where the Fermi-coupling constant is $G_\mu = 1.16637 \cdot 10^{-5}\text{ GeV}^{-2}$ and the cosine of the weak-mixing angle reads $c_w = M_W/M_Z$.

In table 1 we show the numerical results for the individual $\text{N}^{3/2}\text{LO}$ corrections to the unpolarised cross section, $\Delta\sigma^i = \Delta\sigma_{LR}^i/4$, at various centre-of-mass energies near the W -pair production threshold. In detail, the table contains corrections from interference of single-Coulomb exchange and soft/hard corrections from (34) (third column), from the NLO corrections to the Coulomb-potential (39) (fourth column), from interference of single-Coulomb exchange with decay and residue correction in equations (40) and (48) (fifth and sixth columns) and from the triple-Coulomb correction in (11) (seventh column). The result (49) for the sum of the different contributions is given in the second column. It is also instructive to compare to the size of the

	$\sigma(e^-e^+ \rightarrow \mu^- \bar{\nu}_\mu u \bar{d} X)(\text{fb})$						
\sqrt{s} [GeV]	$\hat{\sigma}^{(3/2)}$	$\Delta\hat{\sigma}^{\text{C}\times[\text{S}+\text{H}]}$	$\Delta\sigma^{\text{NLO-C}}$	$\Delta\sigma^{\text{C}\times\text{decay}}$	$\Delta\sigma^{\text{C}\times\text{res}}$	$\Delta\sigma^{\text{C3}}$	$\Delta\sigma^{\text{C2}}$
158	-0.001	-0.116	0.104	-0.037	0.044	0.004	0.151
161	0.147	-0.321	0.226	-0.091	0.324	0.010	0.437
164	0.811	-0.417	0.393	-0.134	0.965	0.003	0.399
167	1.287	-0.389	0.473	-0.142	1.345	0.001	0.303
170	1.577	-0.354	0.511	-0.142	1.561	0.000	0.246

Table 1: Combined $\text{N}^{3/2}\text{LO}$ corrections (second column) and separate contributions from interference of single-Coulomb exchange with soft and hard corrections (third column), renormalisation of the Coulomb potential (fourth column), interference of decay correction and single-Coulomb exchange (fifth column), interference of residue correction and single-Coulomb exchange (sixth column) and triple-Coulomb exchange (all corrections are without ISR improvement). For comparison the NLO contribution from double-Coulomb exchange (C2, second column) are also shown.

	$\sigma(e^-e^+ \rightarrow \mu^- \bar{\nu}_\mu u \bar{d} X)(\text{fb})$				
\sqrt{s} [GeV]	Born	Born (ISR)	NLO	$\hat{\sigma}^{(3/2)}$	$\sigma_{\text{ISR}}^{(3/2)}$
158	61.67(2)	45.64(2) [-26.0%]	49.19(2) [-20.2%]	-0.001 [-0.0‰]	0.000 [+0.0‰]
161	154.19(6)	108.60(4) [-29.6%]	117.81(5) [-23.6%]	0.147 [+1.0‰]	0.087 [+0.6‰]
164	303.0(1)	219.7(1) [-27.5%]	234.9(1) [-22.5%]	0.811 [+2.7‰]	0.544 [+1.8‰]
167	408.8(2)	310.2(1) [-24.1%]	328.2(1) [-19.7%]	1.287 [+3.1‰]	0.936 [+2.3‰]
170	481.7(2)	378.4(2) [-21.4%]	398.0(2) [-17.4%]	1.577 [+3.3‰]	1.207 [+2.5‰]

Table 2: Two implementations of the $\text{N}^{3/2}\text{LO}$ corrections, which differ by the treatment of initial-state radiation compared to the “exact” Born cross section without (second column) and with (third column) ISR improvement and the NLO EFT result including ISR (fourth column). The relative correction in brackets is given with respect to the Born cross section in the second column.

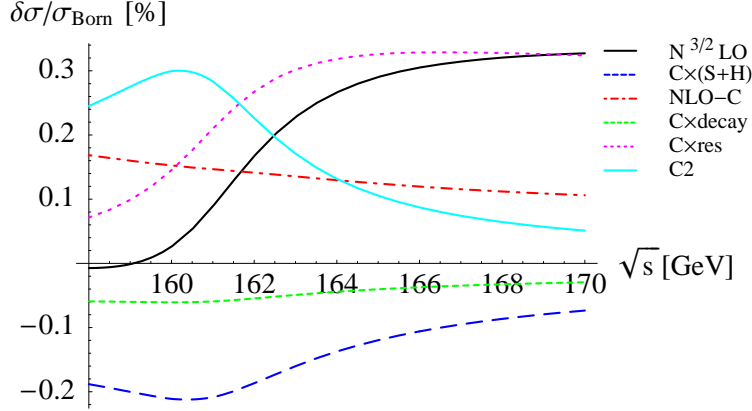


Figure 10: Corrections relative to the Born cross section: Combined $\text{N}^{3/2}\text{LO}$ (solid/black), interference of Coulomb with soft and hard corrections (long-dashed/blue), correction to the Coulomb potential (dash-dotted/red), interference of Coulomb and decay corrections (short-dashed/green) and interference of residue correction and single-Coulomb exchange (dotted/magenta). For comparison the NLO correction from double-Coulomb exchange (light solid/cyan) is also shown.

pure two-Coulomb exchange corrections given by the last term in (10) (eighth column) that also arise from NNLO diagrams in the full theory but appear already at NLO in the EFT power counting. Figure 10 shows the size of the individual corrections and the combined corrections relative to the Born cross section in the full theory computed using a fixed-width prescription. It can be seen that individual corrections are comparable in magnitude to the second Coulomb correction but cancel to a certain extent, in particular in the immediate threshold region where the total $\text{N}^{3/2}\text{LO}$ correction is about one per-mille of the Born cross section. Above threshold the residue correction dominates and the total correction rises to about three per-mille of the Born cross section.

The final results for the $\text{N}^{3/2}\text{LO}$ corrections including ISR improvement (i.e. the result of inserting $\hat{\sigma}^{(3/2)}$ into the convolution with the electron structure functions in (29)) is given in the last column of table 2, together with the previous result without ISR improvement shown in the fifth column. For comparison the Born cross section in the fixed-width prescription with and without ISR improvement generated using WHIZARD [35] and the result of the NLO calculation of [13] (including ISR improvement) are also shown. The ISR improvement is seen to reduce the $\text{N}^{3/2}\text{LO}$ corrections by about 40% at threshold and 25% at 170 GeV. Note that the effect is bigger than in the case of the NLO corrections [13] that are reduced by ISR improvement by about 20% near threshold while there is almost no effect at 170 GeV. We remind the reader that when the $\text{N}^{3/2}\text{LO}$ terms presented here are added to the full 1-loop calculation in the fixed-width or complex-mass scheme [11, 12] (as shown in appendix B, the $\text{N}^{3/2}\text{LO}$ result can be added to the fixed-order NLO result in the complex-mass scheme without modification), the double-Coulomb exchange terms C2 shown in table 2 must also be added,

since these two-loop virtual effects, although part of the NLO EFT calculation shown in table 2, are not included in the fixed-order NLO calculation [11, 12].

In [13] the impact of the interference of single-Coulomb exchange with hard and soft corrections on the W -mass measurement was estimated as $[\delta M_W] \approx -5$ MeV. This expectation was based on a naive estimate for these contributions in eq. (91) of [13] that corresponds to a correction to the cross section of $\Delta\sigma_{\text{est.}}^{3/2}(161\text{GeV}) \sim -0.27\text{fb}$. From table 1 one sees that this correctly captures the order of magnitude of the contribution from interference with soft corrections and hard corrections to the production operator (third column), that is, however, almost completely cancelled by the correction to the Coulomb potential. Adopting the same procedure as in section 6.4 of [13] to estimate the shift of the W mass, however assigning a relative error to each energy point that scales as one over the square root of the expected number of events, we find that the impact of the $N^{3/2}\text{LO}$ corrections on the W -mass measurement is about 3 MeV (5 MeV if the $N^{3/2}\text{LO}$ correction is not convoluted with ISR), smaller than the targeted accuracy. Since other SM NNLO terms are expected to be even smaller, we may conclude that the (partonic) four-fermion cross section near the W -pair production threshold is known with sufficient precision.

5 Towards the experimentally measured cross section

In measurements of the four-fermion production cross section, cuts on momenta or angles of the observed particles have to be applied in order to disentangle signal and background processes. While presently we do not aim at a general treatment of such phase-space cuts using effective-theory methods, we would like to estimate their effect on the corrections calculated in this article.

For orientation, we consider the selection cuts used for the measurement of the four-fermion production cross section at $\sqrt{s} = 161$ GeV at LEP [36, 37, 38, 39]. To be definite, we use the cuts used by the L3 collaboration in [38] to select the $q\bar{q}\mu\nu(\gamma)$ final state that can be summarised as follows:

- (i) The muon momentum has to satisfy $|\vec{p}_\mu| > 20$ GeV;
- (ii) the jet-jet invariant mass M_{jj} and the invariant mass $M_{\mu\nu}$ of the muon-neutrino system have to satisfy $40 \text{ GeV} < M_{jj} < 120 \text{ GeV}$ and $M_{\mu\nu} > 55 \text{ GeV}$, respectively;
- (iii) the angle between muons and both hadronic jets must satisfy $\theta_{\mu j} > 15$ degrees to suppress backgrounds from $q\bar{q}(\gamma)$ production where muons arise as decay products of hadrons;
- (iv) the polar angle of the missing-momentum vector has to satisfy $|\cos \theta_\nu| < 0.95$ to suppress $q\bar{q}(\gamma)$ events where the missing energy arises from a photon lost in the beam pipe.

To discuss the possible effects of these cuts on the $N^{3/2}\text{LO}$ corrections, it has to be understood to which extent they can be incorporated in the effective field theory framework. This will be discussed first for the leading-order cross section before the effect on the radiative corrections is considered.

We have studied the effect of the cuts on the Born cross section in the full SM using WHIZARD [35]. The numerical effects are shown in table 3. These results do not include ISR improvement but we have checked that adding ISR does not change the relative impact of the

Cut	$\sigma_{\text{Born}}(e^-e^+ \rightarrow \mu^-\bar{\nu}_\mu u\bar{d})(\text{fb})$	$\sigma_{\text{cut}}/\sigma_{\text{tot}}$
–	154.18(5)	
$ \vec{p}_\mu > 20 \text{ GeV}$	153.71(5)	99.69(5) %
$M_{\mu\nu} > 55 \text{ GeV}, 40 \text{ GeV} < M_{jj} < 120 \text{ GeV}$	150.61(5)	97.68(5) %
$\theta_{\mu j} > 15 \text{ degrees}$	149.35(5)	96.87(5) %
$ \cos \theta_\nu < 0.95$	148.28(5)	96.17(5) %
all	140.03(5)	90.82(5) %

Table 3: Effects of the phase-space cuts used in [38] on the Born cross section in the full SM at $\sqrt{s} = 161 \text{ GeV}$ without ISR improvement computed using WHIZARD.

cuts. Although individual cuts are not very restrictive, their combined effect reduces the cross section by about 9 percent. The effect of the cut (i) is of the order of three per-mille and will not be considered further. The remaining cuts fall into two categories: the cut (ii) on the invariant masses of pairs of decay products can be implemented in the effective-theory calculation as discussed in subsection 5.1. As shown there, these cuts do not affect the corrections calculated in this article at all. The cuts (iii) and (iv) are sensitive to angular distributions of the decay products of the W bosons and are more problematic in the approach followed in [13] and here. The uncertainty on the theoretical prediction introduced by these cuts is estimated in subsection 5.2.

5.1 Invariant-mass cuts in the effective theory

The precise treatment of invariant-mass cuts on the W -decay products of the form $-\Lambda_1^2 < M_{f_i f_j}^2 - M_W^2 < \Lambda_2^2$ in the effective theory depends on the scaling assigned to the ratio Λ/M_W with respect to the expansion parameter $\delta \sim \Gamma_W/M_W$. For the very loose cuts in (ii) above, it is appropriate to count $\Lambda/M_W \sim 1$ but we find it illuminating to consider also the possibility of tighter cuts of the order $\Lambda/M_W \sim \sqrt{\Gamma_W/M_W} \sim \sqrt{\delta}$.²

To discuss the correct treatment of invariant mass cuts, recall that the total cross section is extracted from appropriate unitarity cuts of the e^-e^+ forward-scattering amplitude [13]. The relevant diagrams receive contributions from W -bosons with potential and hard loop momenta. The potential region contributes starting at LO and is reproduced in the effective theory by the matrix-element of production/destruction operators as shown for leading order in (5), where the W -propagators are given by (7). As long as no soft-photon corrections are considered, the cut on the invariant mass of the decay products translates to cuts on the momenta of the W s circulating in the loop of the form $-\Lambda_1^2 < p_W^2 - M_W^2 < \Lambda_2^2$. These are implemented by inserting a product of step-functions $\theta(\Lambda_2^2 - p_W^2 + M_W^2)\theta(\Lambda_1^2 + p_W^2 - M_W^2)$ in the cut loop integral. We briefly comment on soft photons below. The hard region contributes from N^{1/2}LO and is reproduced in the effective theory by four-electron operators [13]. The effect of invariant mass-cuts in the hard region is included by taking the step functions into account in the calculation of the matching coefficients of the four-electron operators. We now discuss the two different possible scalings assigned to Λ/M_W in turn.

² In this respect it is interesting to mention that in the effective-theory treatment of top-pair production near threshold [40] the assumed hierarchy $\Gamma \ll \Lambda \ll M$ is closer to the second case.

Loose cuts: $\Lambda \sim M_W$ Consider the contribution of the potential region first. Decomposing the W -loop momentum as $p_W = M_W v + r$ with $v = (1, \vec{0})$ and a residual potential momentum $r = (r^0, \vec{r}) \sim (\delta, \sqrt{\delta})$, the step functions implementing the cuts are expanded as $\theta(\Lambda^2 \pm (2M_W r_0 - \vec{r}^2))$. Since by assumption $\Lambda \gg r_0, \vec{r}^2 \sim \delta$ the momentum can be dropped in the step function so that at leading order the cut can be neglected in the loop integrals in the effective theory. In the calculation of the matching coefficients of the four-electron operators, on the other hand, the step functions are operative since the W -loop momenta are hard and taken to be of the order $p_W^2 \sim M_W^2 \sim \Lambda^2$. Therefore a loose cut with $\Lambda \sim M_W$ is taken into account entirely by modifying the matching coefficient of the four-electron operator, while loop integrals in the effective theory are to be performed without constraint on the W -momenta.

Tight cuts: $\Lambda \sim M_W \sqrt{\delta}$ Here the situation is reversed compared to the previous case: in the evaluation of cut loop integrals in the effective theory one has by assumption $|2M_W r_0 - \vec{r}^2| \sim \Lambda^2$, so the step functions have to be taken into account. In the calculation of the matching coefficients of the four-electron operators, the W momenta are taken to be hard and satisfy $|p_W^2 - M_W^2| \gg \Lambda^2$. Since $\theta(\Lambda^2 - |p_W^2 - M_W^2|) \sim \theta(-|p_W^2 - M_W^2|) = 0$, tight cuts lead to vanishing matching coefficients. Therefore the invariant-mass cuts have to be taken into account in the loop calculations in the effective theory, while in the case of tight cuts the four-electron operators do not contribute to the cross section at all. Since $\Lambda^2 \sim M_W \Gamma_W$ some recombination prescription of soft photons and final state fermions has to be supplied.

To verify that the above procedure is the appropriate treatment of invariant-mass cuts in the effective theory, we have computed the full tree-level cross section for the process (1) with symmetric invariant-mass cuts $|M_{u\bar{d}}^2 - M_W^2| < \Lambda^2$, $|M_{\mu\bar{\nu}_\mu}^2 - M_W^2| < \Lambda^2$ using WHIZARD, and compared it to the effective theory cross section obtained using either the counting $\Lambda \sim M_W$ or $\Lambda \sim M_W \sqrt{\delta}$. The result shown in figure 11 shows good agreement with the effective-theory treatment in the regions where the respective counting rule is appropriate. Implementing the cuts of [38] quoted in point (ii) at the beginning of the section by modifying the matching coefficient of the four-electron operator we obtain $\sigma_{\text{EFT}}(161\text{GeV}) = 150.71 \text{ fb}$ in good agreement with the WHIZARD result of $\sigma(161\text{GeV}) = 150.61 \pm 0.05 \text{ fb}$.

We can now address the effect of cuts of the form (ii) on radiative corrections. The discussion above shows that at the order considered here the soft-photon and Coulomb-photon corrections computed in section 3 do not have to be modified by invariant mass cuts as long as they are of the order $\Lambda \sim M_W$. The effects of such cuts on radiative corrections first appears in $N^{3/2}\text{LO}$ contributions to the four-fermion operators which we have not considered in this article since they are included in the NLO four-fermion calculation of [11, 12]. It is nevertheless instructive to consider the expected effect using the estimate of the correction to the total cross section [13] $\Delta\sigma_{4f}^{(3/2)}(\sqrt{s} = 161\text{GeV}) \sim \alpha^4/(108s_w^8 M_W^2) = 0.74 \text{ fb}$, which is consistent with the difference of the EFT NLO calculation and [11, 12]. Estimating the effect of the invariant-mass cuts on this contribution to be of the same order of magnitude of the one on the leading-order four-fermion operator, we have

$$\Delta\sigma_{4f}^{(3/2)} \left(1 - \frac{\Delta\sigma_{4f,\text{cut}}^{(1/2)}}{\Delta\sigma_{4f}^{(1/2)}} \right) \sim 0.03 \text{ fb}. \quad (52)$$

Clearly the effect of the cut is totally negligible.

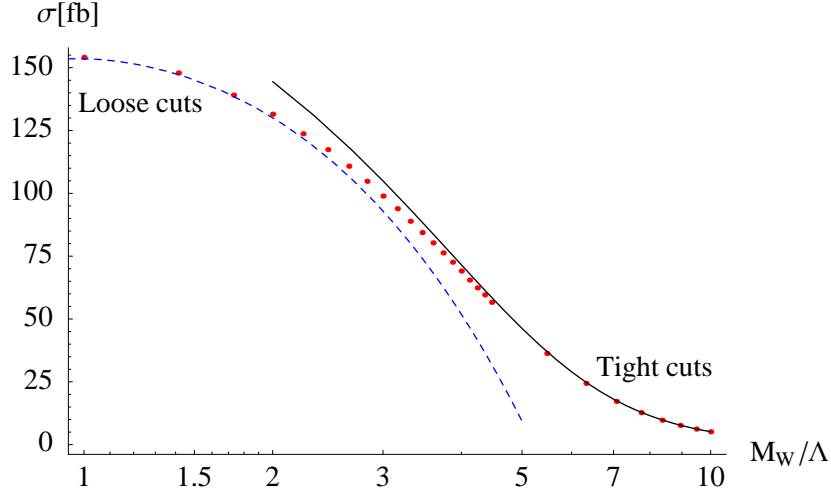


Figure 11: Comparison of the Born cross section in the full SM computed with WHIZARD (red dots) with the effective-theory result for loose-cut implementation (dashed blue curve) and tight-cut implementation (solid black curve).

5.2 Estimating the effect of angular cuts

To discuss the treatment of cuts that involve angles between final state particles such as (iii) and (iv) in the effective-theory framework we will first consider the effect of a cut on the angle between a final-state particle and the beam pipe such as (iv) on the leading-order EFT description before we estimate the effect on the corrections computed in the present paper.

To discuss the effect of angular cuts we can use a variant of the effective theory that includes the decay products [28]. In the leading-order effective-theory description the W bosons are produced in a s -wave by the operator (6). At this order the angular distribution of the W s is predicted to be isotropic. Due to spin correlations the decay-product distributions are not isotropic, and an explicit calculation gives (we consider for definiteness the neutrino angular distribution)

$$\frac{1}{\sigma_{\text{EFT}}^{(0)}} \frac{d\sigma_{\text{EFT}}^{(0)}}{d\cos\theta_\nu} = \frac{3}{16}(1 - \cos\theta_\nu)(3 + \cos\theta_\nu). \quad (53)$$

Computing the effect of the cut (iv) using (53) gives a result $\kappa = \sigma_{\text{EFT, cut}}^{(0)}/\sigma_{\text{EFT}}^{(0)} = 96.16\%$ which is in very good agreement with the number given in table 3. As another example, consider the neutrino forward-backward asymmetry $|(\sigma(\cos\theta_\nu > 0) - \sigma(\cos\theta_\nu < 0))|/\sigma_{\text{tot}} = 3/8$ computed from (53) as compared to the result $\sim 30\%$ obtained using WHIZARD.

A closer look at the angular distributions generated by WHIZARD reveals some deviations from the theoretical leading-order results, for example a forward-backward asymmetry of the W -bosons $|(\sigma(\cos\theta_W > 0) - \sigma(\cos\theta_W < 0))|/\sigma_{\text{tot}} \sim 30\%$. These deviations are mainly to be attributed to non-resonant momentum configurations that are incorporated in the four-fermion operators that are formally of order $N^{1/2}\text{LO}$. At threshold the effect of the four-fermion operators is about 40 percent of the leading order EFT contributions [13], which is consistent with the order of magnitude of the observed asymmetries. The WHIZARD results show an

isotropic distribution of the W s if at the same time invariant mass-cuts in the ‘tight-cut’ regime are applied where the four-electron operators vanish, as shown in section 5.1

Turning to the corrections computed in this paper, we first note that the Coulomb correction neither modifies the angular distribution nor the polarization of the W bosons. The same is true for the one-loop corrections to the production operator $C_{p,LR}^{(1)}$ and the hard-collinear corrections considered in section 3.3 that can be both factorized from the Coulomb Green function. Therefore for all corrections considered in this paper apart from the soft corrections computed in section 3.2 the effect of the angular cuts will be the same as for the leading-order result. Since the numerical effect of the $N^{3/2}$ LO corrections on the total cross section is in the one to three per-mille range, the effect of the angular cuts (which reduce the cross section by about 7 percent) on these corrections will be completely negligible.

We expect that this conclusion is not significantly changed by the soft corrections. First, the components of the momentum of the soft emitted photon are $O(\Gamma_W)$ (see (3)), whereas the momenta of the incoming and outgoing fermions are collinear with an energy of $O(M_W)$. Also the soft photons couple to collinear fermions with eikonal vertices $\sim k^\mu$, that do not change the polarization of the particle the photon is attached to. Even if these arguments would underestimate the effect, the numerical results in the fourth column of table 1 show that a 10 per-cent uncertainty on the effect of the cuts on the soft corrections translates to an uncertainty of the cross section much below 0.1 fb and is therefore not relevant for the desired accuracy needed for the mass measurement. In summary, while a fully differential calculation of the $N^{3/2}$ LO corrections with the EFT method is not currently possible, the mild cuts relevant to the W mass measurements together with the smallness of the correction allow us to conclude that adding the inclusive $N^{3/2}$ LO cross section estimate to the NLO result is sufficient in practice.

6 Conclusions

The aim of this paper has been to ascertain that the four-fermion production cross section near the W -pair production threshold can be calculated with an accuracy that matches the estimated 6 MeV error in the W -mass measurement from an energy scan in e^-e^+ collisions, which requires the consideration of NNLO terms in the Standard Model. The effective field theory approach to unstable-particle production makes it possible to investigate the relevant part of the Standard Model NNLO diagrams without facing the difficulties of a full calculation, which would be overwhelming at present, and to identify a set of parametrically enhanced NNLO corrections, all associated with the strong electromagnetic Coulomb attraction of the intermediate W bosons. We obtain compact analytic expressions for the total cross section, and a result for soft, hard and collinear radiative corrections that extends to the presence of any number of Coulomb photon exchanges. The methods used in this calculation may be useful in other processes involving unstable particles such as top quarks or new heavy states.

We find that individual correction terms to the four-fermion cross section are in the 0.3% range, leading to shifts of the W mass around 5 MeV. However, the combined effect is somewhat smaller. We may thus conclude that the inclusive partonic four-fermion cross section near the W -pair production threshold is known with sufficient precision. We then investigated the impact of cuts, showing how to systematically include invariant-mass cuts into the EFT in two cases differing by the scaling of the cut with the other parameters of the problem. The

cuts applied in the measurement of the W -pair production cross section at LEP2 loose only about 10% of the total cross section. In view of the smallness of the corrections found here, no detailed differential cross section calculations beyond NLO appear to be necessary. Our result should then be combined with NLO calculations of the four-fermion cross section in the SM in the complex mass-scheme [11, 12] as described in appendix B.

The partonic four-fermion cross section must be convoluted with electron structure functions that sum large collinear logarithms. As discussed in [13] to achieve the required precision for the W -mass measurement it will be necessary to improve the treatment of initial-state radiation that was applied at LEP to account consistently for next-to-leading logarithms. This problem is common to all high-precision studies in high-energy e^-e^+ collisions.

Acknowledgement

This work is supported by the DFG Sonderforschungsbereich/Transregio 9 “Computergestützte Theoretische Teilchenphysik”. Feynman diagrams have been drawn with the packages AXODRAW [41] and JAXODRAW [42].

A Renormalisation of the Coulomb potential by hard corrections

In this appendix we discuss several technical aspects related to the hard corrections to the Coulomb potential used in section 3.6 and their dependence on the renormalisation scheme. The calculation of the corrections to the single-Coulomb exchange requires a matching calculation where one computes the renormalised $W^+W^- \rightarrow W^+W^-$ NLO scattering amplitude in the full theory for $(p_1 + p_2)^2 = 4M_W^2$ and compares to the one-loop $\Omega^+\Omega^- \rightarrow \Omega^+\Omega^-$ amplitude in the effective theory. Equivalently, the full-theory calculation can be split into contributions from different momentum regions. The relevant regions are the hard, potential, soft and semi-soft regions. The only contribution that will not be reproduced by diagrams in the EFT is that from the hard region, so for the matching calculation it is sufficient to calculate the hard corrections. At leading order in the non-relativistic expansion only the corrections to the single-Coulomb exchange diagram contribute. In A.1 we define our renormalisation conventions, the hard corrections to the process $W^+W^- \rightarrow W^+W^-$ are discussed in A.2. The relevant results in the $\alpha(M_Z)$ and G_μ input parameter schemes are collected in A.3.

A.1 Charge renormalisation

The lowest perturbative scale relevant near the W -pair production threshold is the W width Γ_W , so we will employ a renormalisation scheme S for the electric charge that is not sensitive to smaller scales, in particular not to the light-fermion masses. In practice we will use $\alpha(M_Z)$ or the Fermi constant G_μ as input parameter (see e.g. [31]), but for the moment we will leave the renormalisation scheme unspecified. Following the renormalisation conventions of [13] the overall one-loop counterterm of the $W^+W^- \rightarrow W^+W^-$ amplitude in the full theory in a given charge-renormalisation scheme S is given by

$$\Delta_{\text{counter}}^S = [\text{tree}] \times (2\delta Z_e^S + 2\delta Z_W), \quad (54)$$

since the tree-level single photon exchange diagram (denoted by [tree]) is proportional to $e^2 = (4\pi\alpha)^2$ and has four external W -legs.

In the following we write the charge counterterm in a given scheme S as the counterterm in the $\alpha(0)$ scheme and a finite scheme-dependent shift

$$\delta Z_e^S = \delta Z_e^{\alpha(0)} - \frac{1}{2}\Delta\alpha^S, \quad (55)$$

with the explicit expressions for the charge counterterm in the $\alpha(0)$ scheme [34]³

$$\delta Z_e^{\alpha(0)} = -\frac{1}{2}\delta Z_{AA} - \frac{s_w}{c_w}\frac{1}{2}\delta Z_{ZA} = -\frac{1}{2}\frac{\partial\Pi_T^{AA}(k^2)}{\partial k^2}\Big|_{k^2=0} + \frac{s_w}{c_w}\frac{\Pi_T^{AZ}(0)}{M_Z^2}, \quad (56)$$

where the transverse self-energies are defined by the decomposition

$$\Pi_{\mu\nu}^{VV}(q) = \left(g_{\mu\nu} - \frac{q_\mu q_\nu}{q^2}\right)\Pi_T^{VV}(q^2) + \frac{q_\mu q_\nu}{q^2}\Pi_L^{VV}(q^2). \quad (57)$$

For the argument given below we assume that light-fermion masses are used as IR regulators in the $\alpha(0)$ scheme, but this will only be used in intermediate steps and the dependence on the light-fermion masses drops out in the end.

A.2 Hard corrections

As discussed at the beginning of this appendix we need to calculate the hard corrections to the $W^+W^- \rightarrow W^+W^-$ amplitude for external momenta directly at threshold. The contributing diagrams are of the form of box corrections (figure 12a), vertex corrections (figure 12b) and self-energy insertions (figure 12c,d). The box corrections with a hard loop momentum do not contribute at the order we are considering since near threshold they are suppressed by a factor v compared to the diagrams with a Coulomb photon. This leaves the vertex and the bubble corrections.

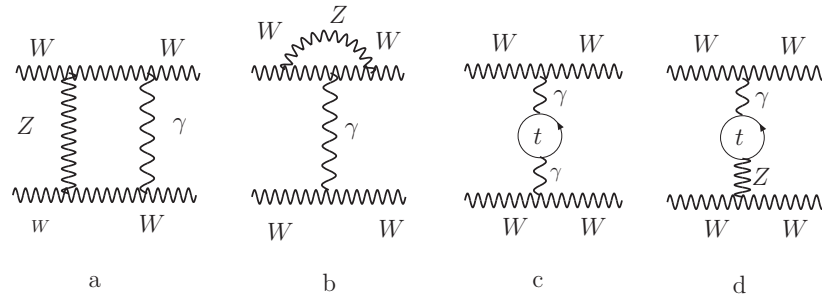


Figure 12: Sample diagrams in the full SM contributing to the hard corrections to the $WW \rightarrow WW$ subprocess

Expanding the vertex-correction diagrams of the form of figure 12b in the region where the photon and the W s attached to the vertex sub-loop are potential and the momentum

³ Here all conventions are the same as in [34] apart from replacing $\Sigma \rightarrow -\Pi$. Note that [34] defines the vacuum polarisation $\Pi_{AA}(k^2) = \Sigma_{AA}(k^2)/k^2$ which we don't use in the following.

running in the vertex loop is hard, one obtains the single-Coulomb exchange diagram with an insertion of the one-loop $WW\gamma$ vertex function evaluated with on-shell external momenta. The renormalised on-shell vertex function vanishes in the conventional on-shell renormalisation scheme where $\alpha(0)$ is used as input parameter.⁴ Therefore the diagrams with insertion of a one-loop *unrenormalised* $WW\gamma$ vertex are given by the negative of the corresponding counterterm in the on-shell renormalisation scheme:

$$\Delta_{\text{vertex}} = [\text{tree}] \times (-2\delta_{WW\gamma}^{os}) = [\text{tree}] \times (-2) \left(\delta Z_e^{\alpha(0)} + \delta Z_W + \frac{1}{2}\delta Z_{AA} - \frac{1}{2}\frac{c_w}{s_w}\delta Z_{ZA} \right). \quad (58)$$

A similar argument shows that in the hard region the self-energies in figures 12c/d are evaluated at zero external momentum. Since the (unrenormalised) one-loop photon self-energy vanishes at zero external momentum the first non-vanishing contributions of diagrams of the form 12c comes from expanding the self-energy to first order:

$$\Delta_\gamma = [\text{tree}] \times (i\Pi_T^{AA,\text{hard}}(k^2)) \frac{-i}{k^2} = [\text{tree}] \times \left(\frac{\partial \Pi_{\text{heavy}}^{AA}(k^2)}{\partial k^2} \Big|_{k^2=0} \right), \quad (59)$$

where Π_{heavy}^{AA} includes all particles except the light fermions. Here it was used that for a hard loop momentum the light-fermion masses must be set to zero so the loop integral is scaleless and only the heavy particles contribute to the hard part of the self-energy at zero external momentum. The unrenormalised photon- Z mixing diagrams give (suppressing the transverse projectors)

$$\begin{aligned} \Delta_{\gamma/Z} &= [\text{tree}] \times 2(i\Pi_T^{AZ}(0)) \frac{-i}{k^2 - M_Z^2} \frac{g_{ZWW}}{g_{\gamma WW}} \\ &\Rightarrow [\text{tree}] \times \left(-2 \frac{\Pi_{T,\text{heavy}}^{AZ}(0)}{M_Z^2} \right) \left(-\frac{c_w}{s_w} \right) = [\text{tree}] \times (\delta Z_{ZA}) \left(-\frac{c_w}{s_w} \right), \end{aligned} \quad (60)$$

since for a potential momentum $k^2 \ll M_Z^2$. Here the on-shell scheme definition $\delta Z_{ZA} = -2\Pi_T^{AZ}(0)/M_Z^2$ has been used. We also used that massless fermion loops do not contribute to the $\gamma - Z$ mixing at zero external momenta, as can be seen from the explicit one-loop result in [34]. Therefore $\Pi_{T,\text{heavy}}^{AZ}(0) = \Pi_T^{AZ}(0)$.

Adding the vertex correction, the γ/Z mixing and the counterterm (54) (where ‘tree’ is again only the photon exchange diagram) one obtains the hard correction in the renormalisation scheme S :

$$\Delta_{\text{hard}}^S = \Delta_{\text{vertex}} + \Delta_\gamma + \Delta_{\gamma/Z} + \Delta_{\text{counter}}^S \equiv [\text{tree}] \times \delta_{\text{hard}}^S, \quad (61)$$

where we defined the correction factor

$$\delta_{\text{hard}}^S = 2(\delta Z_e^S - \delta Z_e^{\alpha(0)}) - \delta Z_{AA} + \frac{\partial \Pi_{\text{heavy}}^{AA}(k^2)}{\partial k^2} \Big|_{k^2=0} = -\Delta\alpha^S - \frac{\partial \Pi_{f \neq t}^{AA}(k^2)}{\partial k^2} \Big|_{k^2=0}. \quad (62)$$

In this expression the derivative of the light-fermion contribution to the photon self-energy depends on light-fermion masses used as regulators in the $\alpha(0)$ scheme. This dependence will

⁴This relies on ‘charge universality’ in the standard model, i.e. on the fact that the on-shell electron-photon vertex and the on-shell W -photon vertex receive the same radiative corrections [43].

be cancelled by a similar term in the conversion factor $\Delta\alpha^S$ for a scheme S that is not sensitive to scales below Γ_W .

Alternatively, the result (62) is obtained by considering the individual renormalised contributions instead of applying the overall counterterm (54). In this case

$$\Delta_{\text{hard}}^S = \Delta_{\text{vertex}}^r + \Delta_\gamma^r + \Delta_{\gamma/Z}^r. \quad (63)$$

Since the on-shell renormalised $Z - \gamma$ mixing two-point function vanishes at zero momentum we have $\Delta_{\gamma/Z}^r = 0$. The renormalised one-loop correction to the $WW\gamma$ vertex vanishes in the on-shell scheme so the only non-vanishing contribution comes from the change in the charge-counterterm:

$$\Delta_{\text{vertex}}^r = 2 [\text{tree}] \times (\delta Z_e^S - \delta Z_e^{\alpha(0)}). \quad (64)$$

The renormalised self-energy correction to the photon-exchange is given by (59) and the corresponding counterterm:

$$\Delta_\gamma^r = [\text{tree}] \times \left(\frac{\partial \Pi_{\text{heavy}}^{AA}(k^2)}{\partial k^2} \Big|_{k^2=0} - \delta Z^{AA} \right). \quad (65)$$

A.3 Formulas for the $\alpha(M_Z)$ and G_μ schemes

We now specialise the result (62) to the two schemes used in the main text. In the $\alpha(M_Z)$ scheme the finite shift of the charge counterterm is given by (see e.g. [34])

$$\Delta\alpha^{M_Z} = -\frac{\partial \Pi_{f \neq t}^{AA}(k^2)}{\partial k^2} \Big|_{k^2=0} + \frac{\text{Re} \Pi_{f \neq t}^{AA}(M_Z^2)}{M_Z^2}. \quad (66)$$

Inserting this definition into (62), the sensitivity on the light-fermion masses drops out and one obtains the final result for the hard corrections to the Coulomb potential (charge counterterm) in the $\alpha(M_Z)$ scheme:

$$\delta_{\text{hard}}^{\alpha(M_Z)} = -\frac{\text{Re} \Pi_{f \neq t}^{AA}(M_Z^2)}{M_Z^2}. \quad (67)$$

In the G_μ scheme the shift in the counterterm is instead given by the correction to muon decay, Δr ,

$$\Delta\alpha^{G_\mu} = \Delta r = -\frac{\partial \Pi_T^{AA}(k^2)}{\partial k^2} \Big|_{k^2=0} - 2 \frac{\delta s_w}{s_w} - 2 \frac{c_w}{s_w} \frac{\Pi_T^{AZ}(0)}{M_Z^2} - \frac{\Pi_T^W(0) - \text{Re} \Pi_T^W(M_W^2)}{M_W^2} + \delta r, \quad (68)$$

$$\frac{\delta s_w}{s_w} = \frac{1}{2} \frac{c_w^2}{s_w^2} \left(\frac{\text{Re} \Pi_T^W(M_W^2)}{M_W^2} - \frac{\text{Re} \Pi_T^Z(M_Z^2)}{M_Z^2} \right), \quad (69)$$

$$\delta r = \frac{\alpha}{4\pi s_w^2} \left(6 + \frac{7 - 4s_w^2}{2s_w^2} \ln c_w^2 \right). \quad (70)$$

The explicit result for the hard corrections in the α_{G_μ} scheme from (62) reads

$$\begin{aligned} \delta_{\text{hard}}^{G_\mu} &= -\Delta r - \frac{\partial \Pi_{f \neq t}^{AA}(k^2)}{\partial k^2} \Big|_{k^2=0} \\ &= \frac{\partial \Pi_{\text{heavy}}^{AA}(k^2)}{\partial k^2} \Big|_{k^2=0} + 2 \frac{\delta s_w}{s_w} + 2 \frac{c_w}{s_w} \frac{\Pi_T^{AZ}(0)}{M_Z^2} + \frac{\Pi_T^W(0) - \text{Re} \Pi_T^W(M_W^2)}{M_W^2} - \delta r. \end{aligned} \quad (71)$$

To convert the result from the $\alpha(M_Z)$ scheme to the G_μ scheme we have to add

$$\begin{aligned} \delta_{\alpha(M_Z) \rightarrow G_\mu} = & \delta_{\text{hard}}^{G_\mu} - \delta_{\text{hard}}^{\alpha(M_Z)} = \frac{\text{Re} \Pi_{f \neq t}^{AA}(M_Z^2)}{M_Z^2} + \frac{\partial \Pi_{\text{heavy}}^{AA}(k^2)}{\partial k^2} \Big|_{k^2=0} \\ & + 2 \frac{\delta s_w}{s_w} + 2 \frac{c_w}{s_w} \frac{\Pi_T^{AZ}(0)}{M_Z^2} + \frac{\Pi_T^W(0) - \text{Re} \Pi_T^W(M_W^2)}{M_W^2} - \delta r. \end{aligned} \quad (72)$$

Explicit expressions for the self-energies appearing in these quantities can be found for instance in [34].

B Conversion to the complex-mass scheme

In the main text we describe the calculation of those $N^{3/2}\text{LO}$ correction in the EFT framework, which are not already included in a NLO calculation in the full Standard Model. The implicit assumption is that the NLO diagram corresponding to exchange of a single (Coulomb) photon between the W bosons is calculated in the on-shell scheme and defined with a fixed-width prescription for the W propagators.⁵ Here we discuss the changes that should be made, if this diagram is calculated as part of a complete NLO SM calculation in the complex-mass scheme defined as in [11, 12].

Since the complex-mass scheme uses the same W -propagators as the fixed-width scheme, the differences arise only from the different renormalisation conventions for α_{ew} and α , and the different treatment of $\Pi^{(1,1)}$ from W -field renormalisation. The different coupling definitions lead to a change in the value of $c_{p,LR}^{(1,\text{fin})}$ in the $C \times H$ correction (20) and an additional term involving $\delta_{G_\mu \rightarrow \alpha_{\text{CMS}}}$ in the NLO Coulomb potential term (39). These compensate exactly for the difference between the coupling prefactors $\alpha_{ew}^2 \alpha$ in the single-Coulomb exchange diagrams in the complex-mass scheme and the G_μ scheme. Thus when the NLO SM calculation is done in the complex-mass scheme, we must add

$$\Delta \sigma_{LR}^{C1} - [\Delta \sigma_{LR}^{C1}]_{\text{CMS}} \quad (73)$$

expanded to order $\alpha_{ew}^2 \alpha^2$ to the $N^{3/2}\text{LO}$ calculation performed in the main text. However, at the indicated order the correction (73) actually vanishes. To see this, extract the relevant coupling constants from the LO scattering amplitude for four-fermion production $\mathcal{A}^{(0)} \equiv \alpha_{ew} \tilde{\mathcal{A}}^{(0)}$, and the amplitude including single-Coulomb exchange, $\mathcal{A}^{(1/2),C1} \equiv \alpha_{ew} \alpha \tilde{\mathcal{A}}^{(1/2),C1}$. The correction to the cross section then involves the quantity

$$2 \text{Re} \left[\mathcal{A}^{(0)} \left(\mathcal{A}^{(1/2),C1} \right)^* \right] = 2 |\alpha_{ew}|^2 \text{Re} \left[\alpha^* \tilde{\mathcal{A}}^{(0)} \left(\tilde{\mathcal{A}}^{(1/2),C1} \right)^* \right]. \quad (74)$$

In the implementation of the complex-mass scheme of [12] the imaginary part of the electromagnetic charge arises only through complex masses entering loop integrals in the charge counterterm. Therefore the imaginary part of α involves terms of the form $\alpha^2 \text{Im}[\log((M_W^2 - iM_W \Gamma_W)/\mu^2)] \sim \alpha^2 \Gamma_W/M_W \sim \alpha^2 \alpha_{ew}$ and does not contribute at order $\alpha_{ew}^2 \alpha^2$ in (73) due to the extra factor of $\Gamma_W/M_W \sim \alpha_{ew}$. Similarly the difference between α_{ew}^2 and $|\alpha_{ew}|^2$ is of higher order, $\alpha_{ew}^2 (\Gamma_W/M_W)^2 \sim \alpha_{ew}^4$.

⁵Since all $N^{3/2}\text{LO}$ corrections calculated in the paper are $O(\alpha)$ corrections to the NLO diagram with a single-Coulomb photon, other NLO diagrams are not relevant.

A change in the renormalisation convention that changes the renormalised value of $\Pi^{(1,1)}$ affects the calculation of the residue correction, but also the value of $c_{p,LR}^{(1,\text{fin})}$ and the NRQED $WW\gamma$ vertex, which depend on the W -field renormalisation convention. The two exactly compensate each other as can be seen as follows: a change in the real part of $\Pi^{(1,1)}$ changes the residue correction by an amount that is directly proportional to $\Delta\sigma_{LR}^{C1}$, as is the term from the change of $c_{p,LR}^{(1,\text{fin})}$, so the cancellation is obvious. A change in the imaginary part of $\Pi^{(1,1)}$ is more subtle, since it affects the imaginary part of $c_{p,LR}^{(1,\text{fin})}$. We dropped this imaginary part in the on-shell scheme, since it does not correspond to cuts involving the four-fermion final state, but this is no longer correct if the field renormalisation is complex. In this case one must include the imaginary part of $c_{p,LR}^{(1,\text{fin})}$ that comes from $\Pi^{(1,1)}$, in which case the $C \times H$ correction is no longer proportional to $\Delta\sigma_{LR}^{C1}$. Rather, as in the calculation of the residue correction, one obtains the integral (47). We thus see again that the change in $\Pi^{(1,1)}$ is compensated by the one in $c_{p,LR}^{(1,\text{fin})}$. A similar argument applies to the change in the $WW\gamma$ vertex. Hence no further correction is needed to convert our result to the case when the full NLO calculation is done in the complex-mass scheme.

References

- [1] The LEP collaborations ALEPH, DELPHI, L3, OPAL and the LEP Electroweak Working Group, *A combination of preliminary electroweak measurements and constraints on the Standard Model*, hep-ex/0612034.
- [2] J.A. Aguilar-Saavedra *et al.* [ECFA/DESY LC Physics Working Group], *TESLA technical design report, part III: physics at an e^+e^- linear collider*, hep-ph/0106315.
- [3] A. Tonazzo and K. Mönig, *Measurement of M_W with direct reconstruction*, talk given by K. Mönig at the *6th workshop on 2nd ECFA/DESY study on physics and detectors for a linear electron-positron collider*, Padova, Italy, 2000. Slides available at <http://www.pd.infn.it/ecfa/>
- [4] G.W. Wilson, *Precision measurement of the W mass with a polarised threshold scan at a linear collider*, DESY LC note LC-PHSM-2001-009. Available at <http://www-flc.desy.de/lcnotes/>
- [5] M. Lemoine and M.J.G. Veltman, Nucl. Phys. B **164** (1980) 445.
- [6] W. Beenakker, F.A. Berends and A.P. Chapovsky, Nucl. Phys. B **548** (1999) 3, hep-ph/9811481.
- [7] A. Denner, S. Dittmaier, M. Roth and D. Wackeroth, Phys. Lett. B **475** (2000) 127, hep-ph/9912261.
- [8] A. Denner, S. Dittmaier, M. Roth and D. Wackeroth, Nucl. Phys. B **587** (2000) 67, hep-ph/0006307.
- [9] S. Jadach, W. Placzek, M. Skrzypek, B.F.L. Ward and Z. Was, Phys. Rev. D **65** (2002) 093010, hep-ph/0007012.

- [10] S. Jadach, W. Placzek, M. Skrzypek, B.F.L. Ward and Z. Was, *Comput. Phys. Commun.* **140** (2001) 432, hep-ph/0103163.
- [11] A. Denner, S. Dittmaier, M. Roth and L.H. Wieders, *Phys. Lett. B* **612** (2005) 223, hep-ph/0502063.
- [12] A. Denner, S. Dittmaier, M. Roth and L.H. Wieders, *Nucl. Phys. B* **724** (2005) 247, hep-ph/0505042.
- [13] M. Beneke, P. Falgari, C. Schwinn, A. Signer and G. Zanderighi, *Nucl. Phys. B* **792** (2008) 89, arXiv:0707.0773 [hep-ph].
- [14] M. Beneke, A.P. Chapovsky, A. Signer and G. Zanderighi, *Phys. Rev. Lett.* **93** (2004) 011602, hep-ph/0312331.
- [15] M. Beneke, A.P. Chapovsky, A. Signer and G. Zanderighi, *Nucl. Phys. B* **686** (2004) 205, hep-ph/0401002.
- [16] A.P. Chapovsky, V.A. Khoze, A. Signer and W.J. Stirling, *Nucl. Phys. B* **621** (2002) 257, hep-ph/0108190.
- [17] W.M. Yao *et al.* [Particle Data Group], *J. Phys. G* **33** (2006) 1.
- [18] A. Sirlin, *Phys. Rev. Lett.* **67** (1991) 2127.
- [19] M. Beneke and V.A. Smirnov, *Nucl. Phys. B* **522** (1998) 321, hep-ph/9711391.
- [20] A. Pineda and J. Soto, *Phys. Rev. D* **59** (1999) 016005, hep-ph/9805424.
- [21] E.H. Wichmann and C.H. Woo, *J. Math. Phys.* **2** (1961) 178.
- [22] M. Beneke, *Perturbative heavy quark-antiquark systems*, contribution to the *8th international symposium on heavy-flavor physics (Heavy Flavors 8)*, Southampton, England, 1999, hep-ph/9911490.
- [23] V.S. Fadin, V.A. Khoze and A.D. Martin, *Phys. Lett. B* **311** (1993) 311.
- [24] V.S. Fadin, V.A. Khoze, A.D. Martin and W.J. Stirling, *Phys. Lett. B* **363** (1995) 112, hep-ph/9507422.
- [25] C.W. Bauer, S. Fleming, D. Pirjol and I.W. Stewart, *Phys. Rev. D* **63** (2001) 114020, hep-ph/0011336.
- [26] C.W. Bauer, D. Pirjol and I.W. Stewart, *Phys. Rev. D* **65** (2002) 054022, hep-ph/0109045.
- [27] M. Beneke, A.P. Chapovsky, M. Diehl and Th. Feldmann, *Nucl. Phys. B* **643** (2002) 431, hep-ph/0206152.
- [28] M. Beneke, N. Kauer, A. Signer and G. Zanderighi, *Nucl. Phys. Proc. Suppl.* **152** (2006) 162, hep-ph/0411008.
- [29] M. Skrzypek, *Leading logarithmic calculations of QED corrections at LEP*, Ph.D. thesis, Jagellonian University, Krakow, Poland, 1992, *Acta Phys. Polon. B* **23** (1992) 135.

- [30] W. Beenakker *et al.*, *WW cross-sections and distributions*, in *Physics at LEP2*, vol. 1, edited by G. Altarelli, T. Sjostrand and F. Zwirner (1996) 79, and CERN yellow report CERN-96-01, hep-ph/9602351.
- [31] S. Dittmaier and M. Krämer, Phys. Rev. D **65** (2002) 073007, hep-ph/0109062.
- [32] S. N. Gupta and S. F. Radford, Phys. Rev. D **24** (1981) 2309; Phys. Rev. D **25** (1982) 3430.
- [33] S. Titard and F. J. Yndurain, Phys. Rev. D **49** (1994) 6007, hep-ph/9310236.
- [34] A. Denner, Fortsch. Phys. **41** (1993) 307, arXiv:0709.1075 [hep-ph].
- [35] W. Kilian, Th. Ohl and J. Reuter, arXiv:0708.4233 [hep-ph].
- [36] K. Ackerstaff *et al.* [OPAL Collaboration], Phys. Lett. B **389** (1996) 416.
- [37] P. Abreu *et al.* [DELPHI Collaboration], Phys. Lett. B **397** (1997) 158.
- [38] M. Acciarri *et al.* [L3 Collaboration], Phys. Lett. B **398** (1997) 223.
- [39] R. Barate *et al.* [ALEPH Collaboration], Phys. Lett. B **401** (1997) 347.
- [40] A. Hoang, Talk given at the International Linear Collider Workshop (LCWS07 and ILC07), Hamburg, Germany, 30 May - 3 Jun 2007; A. Hoang, C. Reisser, P. Ruiz-Femenia, in preparation; P. Ruiz-Femenia, private communication.
- [41] J.A.M. Vermaseren, Comput. Phys. Commun. 83 (1994) 45.
- [42] D. Binosi and L. Theussl, Comput. Phys. Commun. 161 (2004) 76, hep-ph/0309015.
- [43] M. Böhm, A. Denner and H. Joos, “*Gauge theories of the strong and electroweak interaction*,” Teubner Verlag, Stuttgart, Germany (2001) 784 p.